

See discussions, stats, and author profiles for this publication at: <https://www.researchgate.net/publication/259060366>

# Acoustical resonances of assorted ancient structures

Article in *The Journal of the Acoustical Society of America* · February 1996

DOI: 10.1121/1.414642

CITATIONS

64

READS

2,383

3 authors, including:



**Paul Devereux**

Time & Mind Journal, Routledge

22 PUBLICATIONS 222 CITATIONS

[SEE PROFILE](#)



**Michael Ibison**

Texas Garden Shed Foundation

59 PUBLICATIONS 471 CITATIONS

[SEE PROFILE](#)

Some of the authors of this publication are also working on these related projects:



Peer review [View project](#)



Foundations of Electrodynamics [View project](#)

# Acoustical Resonances of Assorted Ancient Structures

*Robert G. Jahn*

Princeton University  
Princeton, New Jersey

*Paul Devereux*

Penzance, United Kingdom

*Michael Ibison*

Princeton University  
Princeton, New Jersey

INTERNATIONAL  
**CONSCIOUSNESS RESEARCH**  
LABORATORIES

ICRL REPORT #95.1

## Acoustical Resonances of Assorted Ancient Structures

Robert G. Jahn, Princeton University  
Paul Devereux, Penzance, United Kingdom,  
Michael Ibison, Princeton University

Princeton Engineering Anomalies Research  
School of Engineering and Applied Science  
Princeton University  
Princeton, NJ 08544-5263

This research is a collaborative project of the International Consciousness Research Laboratories (ICRL), a consortium of several research groups from various countries and academic disciplines, committed to interdisciplinary study of the role of consciousness in the behavior of certain physical systems and processes.

Technical Report PEAR 95002  
March 1995

## Abstract

Rudimentary acoustical measurements performed inside six diverse Neolithic and Iron Age structures revealed that each sustained a strong resonance at a frequency between 95 and 120 Hz (wavelength  $\sim 3$  m). Despite major differences in chamber shapes and sizes, the resonant modal patterns all featured strong antinodes at the outer walls, with appropriately configured nodes and antinodes interspersed toward the central source. In some cases, interior and exterior rock drawings resembled these acoustical patterns. Since the resonant frequencies are well within the adult male voice range, one may speculate that some forms of human chanting, enhanced by the cavity resonance, were invoked for ritual purposes.

## Experimental Design

On an earlier informal tour of certain Anazasi sites in the U. S. Southwest, the authors were struck by the acoustical resonances of various kivas and other ceremonial facilities, and mused whether similar properties might prevail in the more primitive structures that abound in the United Kingdom. To assess such possibilities empirically, a modest itinerary, rudimentary equipment package, and simple protocol were assembled to constitute a pilot experiment that was carried out over a ten-day period in mid-July, 1994. The sites visited are detailed in Table 1.

The equipment deployed consisted of a unidirectional speaker (Realistic #40-1352) driven by a variable frequency sine-wave oscillator (B & K, Precision) enhanced by a 20-watt amplifier (Radio Shack MPA-30, #32-2034), with sound frequency verified by an external, hand-held digital multimeter (Extech TMT-3885, #380285). The sound amplitude patterns were mapped by a portable meter (Realistic #33-2050), sensitive between 55 and 105 dB, sound pressure level, (SPL). In a typical experiment, the source was placed on the floor or on a short tripod roughly at the center of the chamber configuration. The frequency was slowly swept through the lower audible range until the lowest natural resonance of the cavity was evidenced by clearly discernible reverberation of the chamber. With this established, the sound intensity was adjusted to the highest comfortable level, usually between 100 and 110 dB, SPL at the source, and horizontal surveys of sound level were made over some accessible grid covering the chamber. In some cases, vertical or inclined profiles were also attempted.

Table 1 - Ancient Ritual Sites Studied

<u>Site</u>	<u>Location</u>	<u>Age</u>	<u>Configuration</u>
Wayland's Smithy	Berkshire, U.K.	c. 3500 BC	5 m crucifix chamber inside 55 x 15 m trapezoidal mound
Chun Quoit	Cornwall, U.K.	c. 3500 BC	1.5 x 1.5 x 1.5 m trapezoidal chamber under 3 x 3 m capstone
Cairn Euny	Cornwall, U.K.	c. 400 BC	"Beehive" chamber 5 m diameter x 2.5 m high
Cairn L, Carnbane West	Loughcrew, Co. Meath, Ireland	c. 3500 BC	Irregular array of central chamber, seven sub-chambers, and passage, 6 x 5 x 3 m, inside 135 m diameter mound
Cairn I, Carnbane West	Loughcrew, Co. Meath, Ireland	c. 3500 BC	Roughly elliptical array of seven sub-chambers, central chamber, and passage, 5 x 3.5 m overall, originally inside 55 m diameter mound
Newgrange	Co. Meath, Ireland	c. 3500 BC	6.5 x 6.5 m cruciform chamber reached by 19 m passage, inside 50 m diameter mound

To varying degrees, the completeness and precision of these measurements were severely constrained by the limited times available at the sites, intrusion of tourists, awkwardness of the spaces, and control agency requirements, so that only rudimentary maps could be obtained. Nonetheless, certain features were clearly established:

- 1) Despite the substantial small and large scale irregularities in the boundary walls of these structures, their resonant frequencies were well defined. After very little practice, the experimenters could blind-tune the source frequency to a clearly audible resonance with a reproducibility of  $\pm 1$  or 2 Hz with little ambiguity.
- 2) Although many shapes and sizes of cavity were presented, the resonant frequencies of all of them lay in the range between 95 and 120 Hz.
- 3) In all cases, principal antinodes of resonant standing-wave patterns were established at the outer walls, as would be expected theoretically. The number, configuration, and relative magnitudes of the other antinodes and nodes leading back to the source depended on the particular chamber configuration.
- 4) In some cases, rock art on the chamber walls bore some similarity to the observed standing wave patterns.

## Detailed Results

### Wayland's Smithy, Berkshire, United Kingdom

This cruciform chamber, c. 3500 BC, lies within a 55 m long trapezoidal mound. Each of its sub-chambers is roughly 1.5 x 1.5 x 1.0 m interior size, as is its entrance passage. A 1919 excavation revealed 8 skeletons, including one child. The name of this site derives from folk legend that predicts that if a horse and a piece of silver are left overnight, the spectral "Wayland the Smith" will shoe the animal. Acoustical mapping of this complex suffered from its cramped configuration and our early inexperience with the field equipment and mapping strategies. As shown in Fig. 1, the source was placed on the floor at the center of the cross, and radial surveys were made into the East and West Chambers only. The former, which was the more thoroughly mapped, resonated best at 112 Hz, at which frequency it displayed standing wave antinodes at its entrance orifice and at its far wall, separated by one intermediate node. A secondary resonance was identified at 119 Hz, which featured a third antinode roughly one-third of the way into the chamber, separated from the others by two interior nodes. The West Chamber, which was less thoroughly mapped, appeared to resonate more strongly at 95 Hz, which produced a double antinode pattern akin to that in the East Chamber at 112 Hz. The North, Central and Entrance Chambers were not mapped.

### **Chun Quoit, Cornwall, United Kingdom**

This stone chamber or dolmen, c. 3500 BC, consisting of four inward-leaning slabs supporting a capstone weighing several tons, is roughly 1.5 x 1.5 x 1.5 m interior size and was originally surrounded by a cairn of stone. It is speculated that such dolmens were used as ritual burial sites, and for oracular purposes. Again, because of the limited interior space, only a rudimentary survey could be made, and that only with the source placed near the front wall. (Fig. 2). The antinodes were located at the source and at the far wall, with one node midway between. A vertical survey at the node position revealed a positive intensity gradient up to the ceiling, and some further reinforcement of amplitudes at the interior corners was also observed. The huge capstone of this structure had interesting acoustical properties of its own. When struck with a hard object, it reverberated with an assortment of harmonics based a major fifth chord interval above the chamber resonant frequency.

### **Cairn Euny, Cornwall, United Kingdom**

This corbelled "beehive" chamber is attached to a fogou (underground passage) beneath an Iron Age village, c. 400 BC. The original roof has now been partially capped by zinc sheeting. A small recess, of unknown purpose, faces the short entrance passage. The chamber diameter is roughly 5 m, and its central height about 2.5 m. With the source placed on a short tripod at the center, this structure resonated at 99 Hz, establishing the concentric modal pattern sketched in Fig. 3, with the single node positioned closer to the wall than to the source. The pattern was azimuthally quite uniform, with the exception of the regions near the entrance passage and the recess opposite to it.

### **Cairn L, Carnbane West, Loughcrew, Ireland**

This is one of several chambered stone cairns, c. 3500 BC., usually described as "passage tombs", that are scattered about a ridge of the Loughcrew Hills known locally as "Hill of the Witch". The entire cairn is 135 m in circumference, but its irregularly shaped inner chamber is only about 6 x 5 m, and 3 m high. Its 5 m long entrance passage is oriented toward the southeast, allowing sunrise light to fall on an interior free standing limestone pillar on particular days of the year. The chamber is sectoried into seven sub-chambers by appropriately placed standing stones. One of these sub-chambers contains an exceptional basin and backstone, and some of its walls display exquisitely carved patterns. With the source on a short tripod at the center of the main chamber, eight radial surveys were taken in the horizontal plane of the source, penetrating into each of the sub-chambers and the entrance passage. The profiles and the overall plan view of the modal patterns at the dominant resonance frequency of 110 Hz are sketched in Fig. 4. Each of the shorter sub-

chambers sustained a single antinode at the wall, with its associated node slightly inside the chamber orifice. The one deeper chamber directly opposite the entrance passage displayed two antinodes and two nodes, as sketched. Unfortunately, the pattern along the passage was not mapped much beyond its interior orifice. Vertical traverses up the back walls of the large sub-chamber and the basin sub-chamber were unremarkable.

#### **Cairn I, Carbane West, Louchcrew, Ireland**

This satellite cairn lies a few hundred yards southwest of Cairn L and is of similar configuration to it, albeit smaller in scale, and now roofless. The encompassing mound is about 55 m in diameter, and the overall chamber configuration roughly 4 m in major axis. Again there are seven sub-chambers and excellent wall carvings. Eight radial profiles were mapped outward from the source, with results similar to Cairn L. In this case, all sub-chambers sustained only one antinode at the outer walls, and one interior node (Fig. 5). For the three shorter sub-chambers farthest from the entrance, the nodes formed in the central chamber rather than inside the cells, but otherwise the overall plan pattern closely resembled that of Cairn L.

#### **Newgrange, County Meath, Ireland**

The most impressive of all sites surveyed was this 5500 year old cairn near the Boyne River. It features a remarkable 19 m long entrance passage, again opening to the southeast and floridly decorated with rock art, leading to a 6.5 x 6.5 m cruciform configuration composed of a central chamber and three sub-chambers. Each of the sub-chambers contains a mysterious stone basin, and further magnificent rock art designs. With the sound source at its center on a short tripod, the chamber complex resonated at 110 Hz, at which the standing wave patterns sketched in Fig. 6 were established. Radial traverses into the two shorter sub-chambers each showed two nodes and two antinodes, one at the outer wall, and one near the sub-chamber orifice. The deepest sub-chamber allowed a third node-antinode pair to stand inside itself. The overall plan pattern thus involved a closed node in the central chamber, and a closed antinode near the sub-chamber and passage orifices, progressing into the sub-chamber patterns just mentioned. Equally if not more remarkable was the pattern of standing waves sustained along the entire length of the entrance passage. Despite its comparatively small cross-section (roughly 1 m wide x 2 m high), and the large-and small-scale irregularities of the stones forming its walls and ceiling, some twelve antinode/node pairs could be clearly discerned, extending over its full length from chamber to outside entrance, in a classic sinusoidal pattern akin to that of some gigantic musical wind instrument.

## Theoretical Predictions

In principle, it should be possible to calculate analytically the permitted modal patterns and associated resonant frequencies directly from the known chamber configurations and dimensions, but in practice the major irregularities that now prevail in the various interior surfaces doom this approach to complex numerical simulations. A less ambitious strategy would be to idealize the chamber geometries to permit analytical searches for self-consistent patterns, but even here, the plethora of possible modalities precludes specification of unique solutions without resort to some empirical data. Thus, more practical for our purposes is simply to allow the experimental observations to indicate the particular modalities to be considered, and for these to calculate the expected standing wave patterns and frequencies for comparison with the data. Here we outline the results of a few such attempts for the various sites, now presented in order of increasing complexity. Further details of these calculations are sketched in the Appendix.

### Chun Quoit

The inward slanting walls and slightly tipped ceiling of this dolmen present an interior volume that is trapezoidal in its three cross-sections and is further complicated by stone surface irregularities and the entrance aperture at one corner. For purposes of crude comparison, we idealize the space as a cuboid, 1.5 m x 1.5 m in horizontal cross-section and 1.7 m high. As developed in the Appendix, such a volume should support rectilinear standing wave patterns indexed by three integers  $\{n_x, n_y, n_z\}$ , corresponding to the number of half wavelengths contained between the walls perpendicular to the coordinate. Because of the difficulty of maneuvering the sound detector around this space without obstructing the source, the latter had to be placed on the floor adjacent to the front wall ( $x=0$ ,  $y=l_y/2$ ,  $z=0$ ). Consistent with this placement, the sound patterns mapped showed clear antinodes at the front and back walls ( $x=0$  and  $x=l_x$ ), and a node at the center ( $x = l_x/2$ ), as sketched in Fig. 2. Traverses in the  $y$  and  $z$  directions, although showing some variations, were less unambiguous, suggesting that the dominant mode was  $\{1,0,0\}$ . The idealized resonant frequency computed for this mode is 113 Hz, in good agreement with the measured value of 110 Hz.

## Louchcrew I

The simplest idealization that suggests itself for this uncovered structure is to treat it as a vertical elliptical cylinder, closed on the bottom and open on top, sectorized by eight standing stone partitions. Fortunately, the acoustical wave equation separates in elliptical-cylindrical coordinates, yielding standing wave solutions in the form of Mathieu functions, indexed by  $\{l,m,n\}$  corresponding to the number of radial, azimuthal, and vertical nodes. Given the absence of any clear azimuthal or vertical structure in the measured patterns, we may again focus on modes with only radial variation. (It is tempting to speculate whether the builders purposely aligned the sector stones to suppress the angular modes, leaving a sharper and purer resonant tonality). It should also be noted that the current absence of a ceiling to the chamber distorts the vertical profile as now measured from what would have prevailed in the closed configuration, but even then, given the modest chamber height, it is unlikely that any modes having major vertical variation would have been significant contributors to the pattern. The modality is further specified by the appearance of only one node in the measured radial traverses, (Fig. 5), leaving  $\{1,0,0\}$  as the dominant pattern. The measured dimensions of the chamber are best approximated by a semi-major axis of the ellipse of 2.5 m semi-minor axis of 1.8 m, and height 2.0 m, which yield a theoretical resonant frequency of 106 Hz for this mode. This again agrees well with the observed value of 112 Hz, as does the locus of the principal node at some 0.8 m to 0.9 m from the outer wall.

## Cairn Euny

We idealize this corbelled beehive chamber by a cylinder topped by a hemisphere, both of radius 2.5 m. The former supports cylindrical Bessel function modes in the horizontal plane, modulated by sinusoids in the angular and vertical directions. The upper section requires spherical Bessel functions in the radial direction, sinusoidal angular variations in the horizontal plane and Associated Legendre functions to describe the polar angular variation. Since the experimental traverses indicated little angular variation and showed only a single radial node, it appears that the  $\{1,0,0\}$  modes are dominant in both portions of the chamber and thus should match well at the cylinder/hemisphere interface. The cylindrical function predicts resonance at 84 Hz, the hemispherical pattern at 99 Hz. The resonance observed empirically for the hybrid pattern, 99 Hz, is thus not unreasonable. In addition, the  $\{1,0,0\}$  cylindrical mode predicts that the radial node should stand about 0.9 m from the outer wall, which is well within the error bar of the measured location. (Fig. 3).

## Louchcrew L

Despite its less regular configuration, a similar elliptical approximation can be applied to this composite covered chamber. Using a semi-major axis of 2.4 m and a semi-minor axis of 1.7 m, the  $\{1,0,0\}$  mode computes to a resonant frequency of 112 Hz, which again agrees well with the measured value of 110 Hz. This may be rather fortuitous, however, given the empirical observation of a second node-antinode pair in the north sub-chamber, and the very irregular pattern in the southeast sub-chamber (Fig. 4). A more sophisticated approach must patch together an elliptical mode in the central chamber with appropriate rectilinear modes in the five sub-chambers, requiring that their phase fronts match smoothly at or near the apertures to the sub-chambers. Again relying on the measurements to exclude modes having angular or vertical variations, the best matched configuration turns out to require a node to stand near the sub-chamber entrances matching, as it were, a  $\{1/2, 0, 0\}$  elliptical mode in the central chamber to  $\{1/2, 0, 0\}$  rectilinear modes in the northwest (99 Hz), southwest (119 Hz), and southeast (120 Hz) sub-chambers.

The matches are not so good with the northeast (67 Hz) and north (58 Hz) sub-chambers. Referring to the experimental traverses, Fig. 4, it appears that the northeast sub-chamber, perhaps because of its trapezoidal shape, pulls the matching node plane well inside its aperture, which would, of course, increase its resonant frequency from the computed value. The north chamber pattern may be complicated by the standing stone jutting out from its west wall which may induce the additional antinode at the constriction, disrupting the overall resonance.

## Wayland's Smithy

This cruciform configuration was the first visited, and the acoustical survey was, for several reasons, the least adequate. With the source on the floor of the central chamber, nodes and antinodes were discernible in two of the sub-chambers, as sketched in Fig. 1, but at somewhat different resonant frequencies. Based on the equally crude dimensions of these chambers, the  $\{1,0,0\}$  modes observed therein are reasonable, as are their computed resonant frequencies of 102 and 117 Hz, compared to the observed values of 95 and 112 Hz, respectively.

## Newgrange

From the observed standing-wave patterns, it appears that this cruciform configuration also resonates in a self-consistent combination of an elliptical-cylindrical mode in the central chamber, matched to appropriate rectilinear modes in the surrounding sub-chambers, but with common antinodes positioned near the sub-chamber orifices as sketched in Fig. 6. It may be

noteworthy that five of the interior wall stones are well-aligned to reinforce the principle antinode of the central chamber elliptical pattern at azimuthal positions between the sub-chamber orifices but, as discussed in the Appendix, better agreement with measurements is achieved by considering the central pattern to extend up to the first node in each sub-chamber. Therefore the following modal indexes for the sub-chambers refer to the patterns starting from the nodal surface nearest their entrance. Using major and minor axes of 6.4 m and 4.0 m for the central chamber ellipse yields a resonant frequency for the  $\{3/2,0,0\}$  mode of 103 Hz, respectably close to the measured value of 110 Hz. For the west sub-chamber, where a  $\{3/2,0,0\}$  pattern is observed, the measured depth of 2.2 m yields a computed resonance at 117 Hz. In both the north and east sub-chambers, of depth 0.8 m, a  $\{1/2,0,0\}$  pattern is observed, with corresponding theoretical frequency 108 Hz. This composite pattern thus seems quite coherent.

The long entrance passage presents a fascinating acoustical situation of its own. We would expect that sound waves driven into the passage from the central chamber should propagate, with some attenuation, along the full length, and partially reflect from the exit orifice to establish a decaying longitudinal standing wave pattern throughout. Since the cross section of the tunnel is of the order of 1 m wide x 2 m high over most of its length, and since the free space wavelength associated with 110 Hz is about 3 m, no modes other than  $\{n_x, 0, 0\}$  are likely to appear. For the former, the predicted nodal spacing is simply one-half the free space wavelength, or about 1.5 m, which is essentially that observed. The anticipated attenuation outward along the passage is also confirmed, with a slight recovery of amplitude as the pattern passes under the large entrance capstone.

## Rock Art

The Newgrange and Loughcrew sites present extraordinary and well-known examples of diagrammatic rock etchings conventionally regarded as astronomical, seasonal, or environmental representations<sup>1,2</sup> (cf Fig. 7). In several cases, however, the experimenters were also struck by the similarities of certain sketches with the resonant sound patterns characterizing these chambers. For example, a number of these sketches feature concentric circles, ellipses, or spirals that are not unlike the plan views of the acoustical mappings. In other sketches, sinusoidal or zig-zag patterns resemble the alternating nodes and antinodes found in the radial traverses. Note especially that the two zig-zag trains etched on the corbel at the left side of the west sub-chamber of Newgrange have precisely the same number of "nodes" and "antinodes" as the resonant standing wave pattern we mapped from the chamber center out along the passage (Fig. 6). Similarly, one of the Kerbstones displays a triple zig-zag

above a spot and two concentric circles, which in number and spacing would be accurate representations of the modal patterns radiating from the central chamber into the recesses. Conceivably, the triple spiral configurations sketched on the magnificent entrance stone and elsewhere, could be somewhat more metaphysical representations of the interactive resonances of the three sub-chambers.

## Summary

The experimental data and theoretical analyses presented above constitute little more than a pilot study addressing the hypothesis that certain ancient structures possessed resonant acoustical properties that may have contributed to their functional purposes. The extent to which these features were deliberately engineered into these sites, and their particular utilization, are beyond the scope of this study, but certain suggestive aspects, perhaps worthy of more extensive and precise surveys, have been noted. First, by whatever course of design and construction, all six of the diverse configurations visited sustain clearly discernible acoustical resonances in the vicinity of 110 Hz, well within the male voice range. The dominant standing wave patterns at these frequencies are the principle radial or longitudinal harmonics, with little azimuthal or vertical structure. In a few cases, it appears that various interior standing stones may have been positioned to enhance such resonances, by suppressing unwanted azimuthal modes. At some sites, a number of the rock art drawings bear striking similarities to the plan or longitudinal patterns of these standing wave configurations.

Further pursuit of this hypothesis will require much more detailed and precise mapping of these or similar sites, and extension of the techniques to other locales and eras, to establish the breadth and endurance of such acoustical characteristics. It would also be instructive to search the existing reservoirs of archeological and anthropological understanding for evidence of ancient cultural attention to other acoustical phenomena.

## Appendix

### Analysis of Low Frequency Resonances

#### General formulation

The acoustic potential  $\phi(\mathbf{r},t)$  satisfies the wave equation:

$$\nabla^2 \phi - \frac{1}{c^2} \frac{\partial^2 \phi}{\partial t^2} = 0$$

where  $c$  is the prevailing speed of sound. The local acoustic pressure and velocity are given respectively by  $\partial\phi/\partial t$  and  $\nabla\phi$ , with specific solutions determined by the boundary conditions. In our case the boundaries are static, and therefore  $\phi$  can be decomposed into sinusoidal time-varying components of the form:

$$\phi \sim g(\mathbf{r})\cos(\omega t + \theta)$$

where  $g$  satisfies the reduced wave equation:

$$\nabla^2 g + (\omega/c)^2 g = 0$$

and  $\omega$  is the radian frequency of the acoustic potential. The boundary conditions on  $g$  restrict  $\omega$  to a discrete set of eigenvalues,  $\omega_{\mathbf{m}}$ , which are the resonances of the structure, where  $\mathbf{m}$  is a modal index according to some labeling convention. To these eigenvalues correspond a particular set of spatial variations or modes,  $g_{\mathbf{m}}(\mathbf{r};\omega_{\mathbf{m}})$ , satisfying:

$$\nabla^2 g_{\mathbf{m}} + (\omega_{\mathbf{m}}/c)^2 g_{\mathbf{m}} = 0$$

For stone walls, the appropriate boundary conditions are that the velocity normal to the walls is zero, corresponding to perfect reflection. Where the structure is open (at the entrance, or where there is no roof) the conditions on  $g$  are more complicated and depend on the details of the opening geometry, resulting in partial reflection with phase shift.

In general, an acoustical source inside the structure can excite a number of these modes, so that the acoustic potential is a linear superposition:

$$\phi = \sum_{\mathbf{m}} a_{\mathbf{m}} g_{\mathbf{m}}(\mathbf{r}; \omega_{\mathbf{m}}) \cos(\omega_{\mathbf{m}} t + \theta_{\mathbf{m}})$$

where the relative contributions,  $a_{\mathbf{m}}$ , of the modes to the overall acoustic potential depends on the nature of the source. This model is approximate in presuming that the source is composed entirely of frequency components which are the resonances of the structure. In practice, a source at any frequency may be used to excite the structure, but a fuller treatment would then have to take account of the spatial extent and non-zero impedance of the source, as well as losses in the air, at the walls, or due to the presence of additional matter (such as the human body). However, an idealized source at a particular resonance,  $\omega_{\mathbf{m}}$ , will excite just one mode,  $g_{\mathbf{m}}(\mathbf{r}; \omega_{\mathbf{m}})$ . The acoustic pressure will then be proportional to  $g_{\mathbf{m}}(\mathbf{r}; \omega_{\mathbf{m}}) \sin(\omega_{\mathbf{m}} t)$  and so have the spatial variation of the resonant mode.

Application of this formalism to our particular structures requires a few other ad hoc strategies appropriate to individual situations, as detailed below. In all cases, however, our attention focuses on the lowest frequency members of the theoretically possible resonances, for several reasons. First, the frequencies of these are found to be relatively uniform across sites, compared to the distribution of resonances within sites. Second, since the walls of the structures in question are constructed from roughly hewn stones, the quality of the resonance ( $Q$ ) should fall off rapidly at the higher frequencies. Third, the low range of frequencies is more accessible to human acoustical generation and detection physiology, i.e., the human male voice can generate a relatively high intensity in this range, and the human ear can detect it sensitively and comfortably.

In the following sections, we address the various sites, in order of increasing analytical complexity:

### Chun Quoit

This relatively simple trapezoidal structure has sides of length 1.7 m at the base, decreasing to 1.35 m at the roof which, on average, is about 1.7 m from the base. Clearly, the lowest frequency resonance must be higher than that of a 1.7 m cube, yet lower than that of a 1.35 x 1.35 x 1.7 m cuboid. Since the spatial variation of the modes in rectangular geometries are separable in rectilinear coordinates, an approximate table of resonances can be obtained if the structure is taken to be a cuboid with dimensions  $l_x = 1.5$  m,  $l_y = 1.5$  m,  $l_z = 1.7$  m. Using the mode index  $\mathbf{m} \equiv \{n_x, n_y, n_z\}$  where the  $n_k$  are

positive integers or zero corresponding to independent definition of the modes in the x,y,z directions respectively, the allowed modes are:

$$g_{\mathbf{m}}(\mathbf{r};\omega_{\mathbf{m}}) = \cos\left(\frac{n_x\pi x}{l_x}\right)\cos\left(\frac{n_y\pi y}{l_y}\right)\cos\left(\frac{n_z\pi z}{l_z}\right)$$

where

$$\omega_{\mathbf{m}} = \pi c \left[ \left(\frac{n_x}{l_x}\right)^2 + \left(\frac{n_y}{l_y}\right)^2 + \left(\frac{n_z}{l_z}\right)^2 \right]^{1/2}$$

and  $c$  is the speed of sound. The acoustical sound pressure is proportional to  $g$  and will therefore follow the same spatial variation. Using  $c = 344$  m/s at 293 K here and throughout, the resonant frequencies  $\omega_{\mathbf{m}}/2\pi$  are tabulated below for the first few combinations of  $\{n_x, n_y, n_z\}$ :

Table 2 - Resonant frequencies at Chun Quoit

$n_z$		0			1			2		
$n_y$		0	1	2	0	1	2	0	1	2
$n_x$	0	0	113	225	103	152	248	205	234	305
	1	113	159	252	152	190	272	234	260	325
	2	225	252	319	248	272	335	305	325	379

Note that the lowest frequency modes, (written as  $\{n_x, n_y, n_z; \omega_{\mathbf{m}}/2\pi\}$ ), namely  $\{0,0,1; 103\}$ ,  $\{1,0,0; 113\}$ , and  $\{0,1,0; 113\}$ , are virtually indistinguishable, (with the next closest in frequency being at 152 Hz). Given an isotropic source of about 110 Hz, there is no a priori reason to select any one of these modes in preference to the others, and some combination of these may contribute to the lowest perceived resonance. However, at this and other sites we found very little nodality in the vertical direction, indicating that the best candidates for the low frequency resonance are  $\{1,0,0; 113\}$  and  $\{0,1,0; 113\}$ . Due to placement of the source near the entrance wall, only the former was actually excited.

## Loughcrew I

We approximate the geometry of this structure as a cylinder of elliptical horizontal cross-section. The appropriate co-ordinates for separation of the wave equation are labeled  $r \equiv \{\xi, \zeta, z\}$  where  $\xi, \zeta$  are respectively the 'elliptical radius' and 'elliptical angle', and  $z$  is the vertical direction. The entrance passage can be expected to distort the elliptical phase-fronts somewhat, although the opening is a relatively small fraction of the boundary seen by an elliptical mode and may be neglected when considering modes with little or no variability in the angular ( $\zeta$ ) direction. The radially oriented stones form open sub-chambers around the central chamber of the structure. Because these stones are narrow, each subtends a relatively small angle, and may be neglected for modes with little or no variability in the angular direction. However, they could strongly suppress or distort modes with greater angular variability.

Denoting the mode index  $\mathbf{m} \equiv \{l, m, n\}$ , the full solution is<sup>3</sup>:

$$\begin{aligned} \phi = & \sum_{l=0}^{\infty} \sum_{m=0}^{\infty} \sum_{n=0}^{\infty} a_{l,m,n}^{(+)} \text{Ce}_m(\xi, q_{m,l}^{(+)}) \text{ce}_m(\zeta, q_{m,l}^{(+)}) \cos\left(\frac{n\pi z}{l_z}\right) \cos(\omega_{l,m,n}^{(+)} t) \\ & + \sum_{l=0}^{\infty} \sum_{m=1}^{\infty} \sum_{n=0}^{\infty} a_{l,m,n}^{(-)} \text{Se}_m(\xi, q_{m,l}^{(-)}) \text{se}_m(\zeta, q_{m,l}^{(-)}) \cos\left(\frac{n\pi z}{l_z}\right) \cos(\omega_{l,m,n}^{(-)} t) \end{aligned}$$

where the labels (+) indicate symmetry about the major axis, those labels (-) indicate symmetry about the minor axis. The ce and se are Mathieu functions of the first kind; the Ce and Se are modified Mathieu functions of the first kind<sup>3,4</sup>. The eigenvalues  $q_{m,l}^{(+/-)}$  are determined by the boundary conditions:

$$\begin{aligned} \text{Ce}'_m(\xi_0, q_{m,l}^{(+)}) &= 0 \\ \text{Se}'_m(\xi_0, q_{m,l}^{(-)}) &= 0 \end{aligned}$$

where  $\xi_0$  is the 'elliptical radius' to the walls from the nominal origin:

$$\xi_0 = \cosh^{-1}(1/e)$$

and  $e$  is the eccentricity of the ellipse,  $(1-b^2/a^2)^{1/2}$ , with  $a, b$  and the semi-major and semi-minor axes. The corresponding resonant frequencies are:

$$\omega^{(+/-)}_{l,m,n} = c [ 4q^{(+/-)}_{m,l} / (a^2 - b^2) + (n\pi/l_z)^2 ]^{1/2}$$

For the special case of no horizontal variation, ( $l=0, m=0$ ):

$$Ce'_0(\xi_0, q_{0,0}^{(+)}) = 0 \Rightarrow q_{0,0}^{(+)} = 0;$$

whence

$$Ce_0(\xi, q_{0,0}^{(+)}) = ce_0(\zeta, q_{0,0}^{(+)}) = 1/\sqrt{2}$$

For these modes:  $Ce_0(\xi, q_{0,0}^{(+)})ce_0(\zeta, q_{0,0}^{(+)})\cos\left(\frac{n\pi z}{l_z}\right)\cos(\omega_{0,0,n}^{(+)}t) = \frac{1}{2}\cos\left(\frac{n\pi z}{l_z}\right)\cos(\omega_{0,0,n}^{(+)}t),$

which is symmetric about both major and minor axes. Although Loughcrew I is now roofless, there are indications that a roof existed at around 2.0 m height. Accordingly, we take  $a = 2.5$  m,  $b = 1.8$  m, and  $l_z = 2.0$  m, whence  $e = 0.69$  and  $\xi_0 = 0.91$ . The corresponding resonant frequencies in Hz are listed below.

Table 3 - Resonant Frequencies at Loughcrew I

No horizontal plane variation,  $\omega_{0,0,n}^{(+)} / 2\pi$ :

**n=0** : 0      **n=1** : 86      **n=2** : 172      **n=3** : 258

No angular variation, first radial mode,  $\omega_{1,0,n}^{(+)} / 2\pi$ :

**n=0** : 106      **n=1** : 137      **n=2** : 202      **n=3** : 279

First angular mode, symmetric about major axis,  $\omega_{1,1,n}^{(+)} / 2\pi$ :

<b>n</b>		<b>0</b>	<b>1</b>	<b>2</b>	<b>3</b>
<b>1</b>	<b>0</b>	41	95	177	261
	<b>1</b>	115	143	207	282

First angular mode, symmetric about minor axis,  $\omega_{1,1,n}^{(-)} / 2\pi$ :

<b>n</b>		<b>0</b>	<b>1</b>	<b>2</b>	<b>3</b>
<b>1</b>	<b>0</b>	55	102	180	264
	<b>1</b>	103	134	200	277

If we confine our attention to the modes with no vertical or angular variation, the lowest resonant frequency is {1,0,0; 106}. This mode has an antinode at the source and at the walls, with a single node at  $\xi = 0.5$ .

Using the relations

$$x = ae \cosh(\xi) \cos(\zeta)$$

$$y = ae \sinh(\xi) \sin(\zeta)$$

then on the major axis,  $\xi = 0$ ,  $y = 0$ , the node is predicted to be at  $x = ae \cosh(\xi) = 1.9$  m. The measured resonance at 112 Hz is found to have a node at 2.15 m (traverse H in Fig. 5) and

1.25 m (traverse D is Fig. 5) giving 1.7 m as the symmetrized intersect with the major axis. These results are well within the tolerances, notwithstanding our neglect of the radially oriented stones.

### **Semi-quantitative approximation**

Only for very simple geometries is it possible to obtain exact solutions for the modes and resonances. In order to arrive at some understanding of the acoustical properties of the more complex structures in question, the modes would need to be computed numerically, which is beyond the scope of this study, or some approximate strategy must be adopted. One approximate approach is to partition the structures into sub-chambers each having a simple three-dimensional geometry. These sub-chambers are not completely closed, but share open surfaces with one another. The particular chamber geometries are selected so that their resulting natural modes are expressible in terms of simple functions. This still leaves open the placement of the interface surfaces and the boundary conditions imposed at those interfaces. Clearly, the acoustic potential and its normal derivative must be continuous across the interfaces for all time, which is only possible if the resonant frequencies of the individual sub-chambers agree. We further simplify the problem by demanding that their modes present nodes, or antinodes, on both sides of any interface surface, which automatically ensures that the acoustic potentials or their normal derivatives are continuous across the interfaces.

Strictly, the coupling efficiency between nodes on either side of an interface should be used to test the appropriateness of the choice of nodes. In this simplified approach, we will assume efficient coupling between nodes having a similar resonant frequency, and with qualitatively similar spatial variation across the interface. This approximate technique of mode matching cannot be guaranteed to give all the resonances of the composite structure. However, it seems to work quite well for the three sites to which it has been applied, namely Cairn Euny, Loughcrew L, and Newgrange.

## Cairn Euny

A natural partitioning for this structure is a horizontal plane at the height where the corbelled roof meets the cylindrical base. This makes the base section a cylinder with an open top, of radius 2.5 m and height 2.5 m, and the roof section a hemisphere of radius 2.5 m. The base geometry demands that the wave equation be written in cylindrical polars  $r \equiv \{r, \theta, z\}$  for which the solutions are Bessel functions in the radial direction, and sinusoids in the angular and vertical directions. Labeling the modes  $\mathbf{m} \equiv \{l, m, n\}$ , and keeping a notation similar to the elliptical structure at Loughcrew I, we expand the acoustic potential using real functions of  $\theta$ :

$$\begin{aligned} \phi = & \sum_{l=0}^{\infty} \sum_{m=0}^{\infty} \sum_{n=0}^{\infty} a_{l,m,n}^{(+)} J_m \left( \frac{u_{m,l} r}{a} \right) \cos(m\theta) \cos \left( \frac{n\pi z}{l_z} \right) \cos(\omega_{l,m,n} t) \\ & + \sum_{l=0}^{\infty} \sum_{m=1}^{\infty} \sum_{n=0}^{\infty} a_{l,m,n}^{(-)} J_m \left( \frac{u_{m,l} r}{a} \right) \sin(m\theta) \cos \left( \frac{n\pi z}{l_z} \right) \cos(\omega_{l,m,n} t) \end{aligned}$$

Unlike the elliptical case, here there is only one boundary condition, which at the cylinder walls  $r = a$ , determines the eigenvalues  $u_{m,l}$ :

$$J_m'(u_{m,l}) = 0,$$

where the prime denotes differentiation, whence the resonant frequencies are:

$$\omega_{l,m,n} = c [ (u_{m,l}/a)^2 + (n\pi/l_z)^2 ]^{1/2}.$$

(As for the elliptic structure, the special case of no horizontal variation is subsumed as  $u_{0,0}$ .) Using  $a = 2.5$  m,  $l_z = 2.5$  m, the resonant frequencies  $\omega_{l,m,n}/2\pi$  are listed below.

Table 4 - Resonant frequencies in base partition at Carn Euny

n		0			1			2		
m		0	1	2	0	1	2	0	1	2
1	0	0	41	67	69	80	96	138	143	153
	1	84	117	146	109	136	162	161	181	201
	2	154	186	220	168	198	231	206	231	260

The hemispherical roof portion demands that the wave equation be written in spherical polars,  $r \equiv \{r, \theta, \phi\}$ , corresponding to the radius, the angle in the horizontal plane, and the polar angle respectively. In this geometry the solutions are<sup>1</sup>:

$$\phi = \sum_{l=0}^{\infty} \sum_{m=0}^{\infty} \sum_{n=0}^{\infty} a_{l,m,n}^{(+)} j_n \left( \frac{w_{n,l} r}{a} \right) \cos(m\theta) P_n^m(\cos(\phi)) \cos(\omega_{l,m,n} t) \\ + \sum_{l=0}^{\infty} \sum_{m=0}^{\infty} \sum_{n=0}^{\infty} a_{l,m,n}^{(-)} j_n \left( \frac{w_{n,l} r}{a} \right) \sin(m\theta) P_n^m(\cos(\phi)) \cos(\omega_{l,m,n} t)$$

where the  $j_n$  are spherical Bessel functions<sup>5</sup> of order  $n$ , the  $P_n^m$  are associated Legendre functions<sup>5</sup>, and the boundary condition at the wall  $r=a$  defines the  $w_{n,l}$ :

$$j_n'(w_{n,l}) = 0$$

for which the resonant frequencies are:

$$\omega_{l,m,n} = \frac{c w_{n,l}}{a}$$

Using  $a = 2.5$  m, the resonant frequencies  $\omega_{l,m,n}/2\pi$  in Hz are listed below:

Table 5 - Resonant frequencies in roof partition at Carn Euny

n		0	1	2
1	0	0	46	73
	1	99	132	159
	2	168	201	237

Comparison of Tables 4 and 5 reveals that base mode {1,0,0; 84} and the roof mode {1,0,0; 99} are the lowest frequency resonances for  $m = n = 0$ . These seem sufficiently close to be accepted as candidates for the lowest resonance for the entire structure. Thus applied, this method of partitions reasonably concurs with the measured resonance (99 Hz), and correctly predicts the measured modal pattern. In particular, the node position is predicted to be at the point  $r$  given by

$$J_0\left(\frac{u_{0,0}r}{a}\right) = 0$$

for which

$$\frac{u_{0,0}r}{a} = 2.4$$

Using  $u_{0,0} = 3.83$  gives  $r = 1.6$  m which agrees well with measured values, as shown in Fig. 3.

#### Loughcrew L

We start by considering the whole structure as an elliptical cylinder, just as for Loughcrew I. Clearly, this is a rough approximation to the true structure, and the dimensions we can choose for the major and minor axes are somewhat arbitrary. Using  $a = 2.4$  m,  $b = 1.7$  m,  $l_z = 3.0$  m, giving  $e = 0.71$ ,  $\xi_0 = 0.88$ , the resonant frequencies are listed below.

Table 6 - Resonant frequencies at Loughcrew L - composite structure

No horizontal plane variation,  $\omega_{0,0,n}^{(+)} / 2\pi$ :

n=0 : 0      n=1 : 57      n=2 : 115      n=3 : 172

No angular variation, first radial mode,  $\omega_{1,0,n}^{(+)} / 2\pi$ :

n=0 : 112      n=1 : 126      n=2 : 160      n=3 : 205

First angular mode, symmetric about major axis  $\omega_{1,1,n}^{(+)} / 2\pi$ :

n		0	1	2	3
1	0	42	71	122	177
	1	119	132	165	209

First angular mode, symmetric about minor axis  $\omega_{1,1,n}^{(-)} / 2\pi$ :

n		0	1	2	3
1	0	58	82	129	181
	1	107	122	157	203

Of these, the first radial mode having no vertical variation is {1,0,0; 112} which agrees well with the measured resonance of 110 Hz.

For a more precise solution, we may apply the method of partitions, by choosing surfaces which define each of the ancillary chambers as cuboids. This leaves some freedom in the positioning of the partition planes, and consequently, of the effective dimensions of the central chamber, in acknowledgement of the empirical results. The proposed partition surface corresponds with the nodal contour sketched in Fig. 4. Note that the semi-minor axis is approximately the same length as the depth of the northwest and southwest cavities. Because the acoustic potential must have an anti-node at the walls, it follows that for a radially symmetric mode with an anti-node at the center of the central chamber, we expect

Table 9 - Resonant frequencies in east chamber, at Wayland's Smithy

n		0			1			2		
m		0	1	2	0	1	2	0	1	2
1	0	0	212	424	174	274	658	347	407	548
	1	117	247	440	209	298	473	366	423	560
	2	234	316	484	291	360	514	418	464	596

Consistent with the observed modal structure, the fundamental resonances are  $\{1,0,0; 102\}$  for the west chamber, and  $\{1,0,0; 117\}$  for the east chamber, acceptably close to the measured resonances and modal structure at 95 Hz and 119 Hz, respectively.

#### Newgrange

This cruciform structure also requires the partitioning approach. The natural choice is to represent each of the three arms and the entrance tunnel by cuboids, with the remaining central chamber treated as an ellipse. Due to the relatively long length of the entrance chamber, the boundary conditions at its entrance will have negligible effect on the modes and resonant frequencies of the structure as a whole. Accordingly, we consider initially just the three arms and the central chamber, whose relative dimensions, as defined by the stone walls, suggest using anti-nodal surfaces as the artificial boundary conditions at the partition interfaces. Once again, the choice of location of the partition surface, especially with the North chamber pattern, is dictated by the empirical results. Considering modes with no vertical or lateral variation,  $\mathbf{m} = \{n_x, 0, 0\}$ , the resonant frequencies are listed below.

Table 10 - Resonant frequencies of Newgrange ancillary chambers bounded by anti-nodes

$n_x$ :	1	2	3
chamber (depth)			
E (1.5 m)	115	229	345
N (2.0 m)	86	172	258
W (2.9 m)	59	119	178

For the central chamber, consistent with the chosen ancillary dimensions, we take  $a = 2.0$  m,  $b = 1.2$  m, giving  $e = 0.8$ ,  $\xi_0 = 0.69$ , and  $q_{0,1}^{(+)} = 4.5$ . Unfortunately, the first radially symmetric mode with no vertical variation,  $\{1,0,0; 145\}$ , then has much higher natural frequency than the measured value of 110 Hz, suggesting that the artificial boundaries have been inappropriately placed. We thus must resort to placing the partitions at the next *nodal* surface, despite the fact that it does not coincide with the stones closest to the center of the central chamber. If the dimensions are derived from the empirical results and we still take the ancillary chambers to be cuboids, and if we represent the central chamber, now bounded by the nodal surface, as an elliptical cylinder, then the results for modes with no vertical or lateral variation,  $\mathbf{m} = \{n_x, 0, 0\}$ , are those tabulated below.

Table 11 - Resonant frequencies of Newgrange ancillary chambers bounded by nodes

$n_x$ :	1/2	3/2	5/2
chamber (depth)			
E (0.8 m)	108	323	538
N (0.8 m)	108	323	538
W (2.2 m)	39	117	195

For the central chamber, we now use  $a = 3.2$  m,  $b = 2.0$  m, giving  $e = 0.35$ ,  $\xi_0 = 1.7$ , and apply the modified boundary condition that the acoustical potential is at a node at  $\xi_0$ , which yields  $q_{0,1/2}^{(+)} = 0.3$  and  $q_{0,3/2}^{(+)} = 1.1$ . The two lowest frequency modes are then  $\{1/2, 0, 0; 54\}$  and  $\{3/2, 0, 0; 103\}$ , suggesting an overall resonance of the latter with the ancillary chamber modes E:  $\{1/2, 0, 0; 108\}$ , N:  $\{1/2, 0, 0; 108\}$ , W:  $\{3/2, 0, 0; 117\}$ . This model agrees far better

with the measured resonance at 110 Hz, and with the observed mode structure in the radial traverses.

Acoustic energy at this resonance will also couple into the entrance hall. Some fraction of the power will be reflected from the exit aperture, resulting in a  $\{n_x, 0, 0\}$  standing wave modulated by some decay towards the exit. At 110 Hz, the expected wavelength is 3.13 m, and therefore, over the 17 m from the first node in the hall to the exit, we can predict  $2 \cdot 17 / 3.13 = 10.8$  node-to-node transitions in the standing wave pattern. This corresponds well to the measured number of 10.5.

## Acknowledgements

The authors are indebted to those agencies in the British Isles who provided access to, and information about, the various sites studied, most notably the National Monuments Branch of the Office of Public Works, Ireland, for special arrangements with respect to Newgrange. We also appreciate the assistance of Mr. John Bradish in designing and assembling the field equipment, and of Ms. Charla Devereux and Ms. Brenda Dunne in performing the field experiments. This work was supported by a grant from the Fetzer Institute.

## References

1. C. O'Kelly: "Concise Guide to Newgrange", C. O'Kelly, Cork, Ireland (1993).
2. N. L. Thomas: "Irish Symbols of 3500 B.C.", Mercier Press, Dublin (1988).
3. N. W. McLachlan: "Theory and Application of Mathieu Functions", Dover (1964).
4. M. Abramowitz, I. Stegun: "Handbook of Mathematical Functions", Dover (1970).
5. L. I. Schiff: "Quantum Mechanics", McGraw-Hill (1968).

## List of Illustrations

- Figure 1:      Wayland's Smithy  
                 Photograph of site  
                 Plan view of modal pattern\*  
                 Traverses S-A and S-B
- Figure 2:      Chun Quoit  
                 Photograph of site  
                 Plan view of modal pattern  
                 Traverses S-A (floor) and S-B (ceiling)
- Figure 3:      Cairn Euny  
                 Photograph of site  
                 Plan view of modal pattern  
                 Traverses S-A through S-J
- Figure 4:      Louchcrew Cairn L  
                 Photograph of site  
                 Plan view of modal pattern  
                 Traverses S-A through S-G
- Figure 5:      Louchcrew Cairn I  
                 Photograph of site  
                 Plan view of modal pattern  
                 Traverses S-A through S-H
- Figure 6:      Newgrange  
                 Photograph of site  
                 Plan view of modal pattern in cruciform chamber  
                 Traverses S-A, S-B, S-C  
                 Plan view of modal pattern in tunnel  
                 Traverse S-D
- Figure 7:      Rock Art Photographs

\* In all plan view modal patterns, node contours are denoted by  $\text{---}\nabla\text{---}$ ; antinode contours by  $\text{---}O\text{---}$ . Source position is denoted by S.

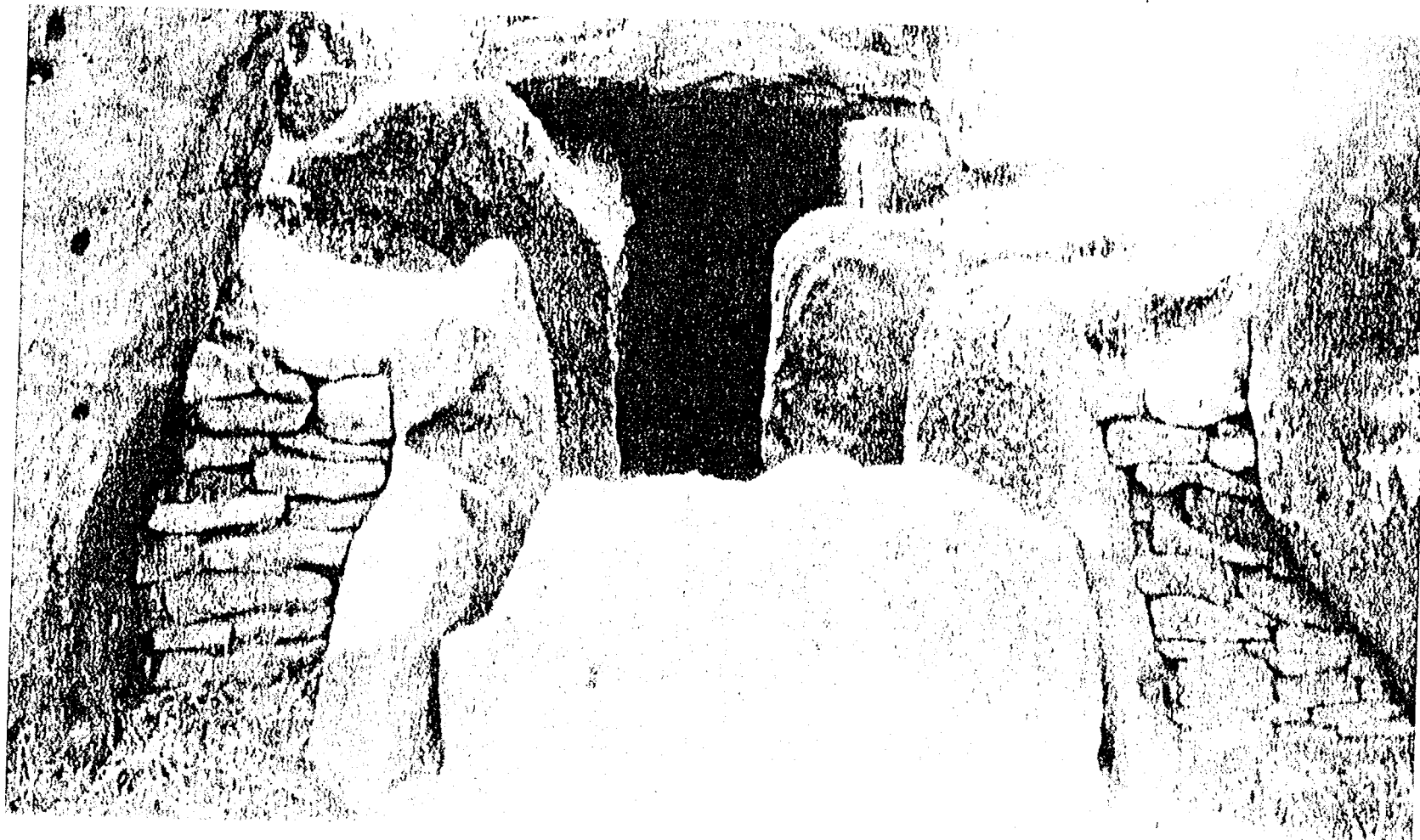
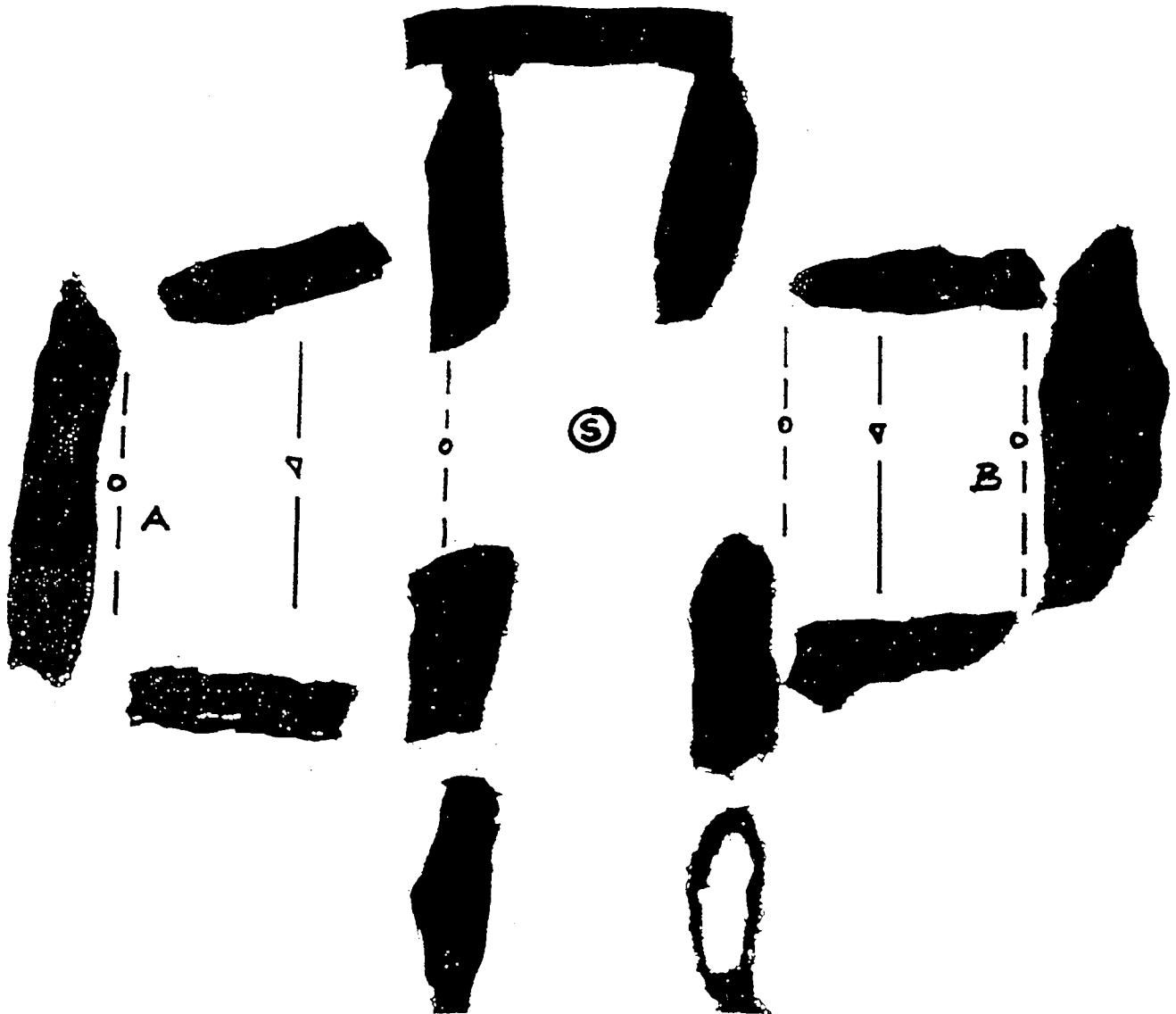
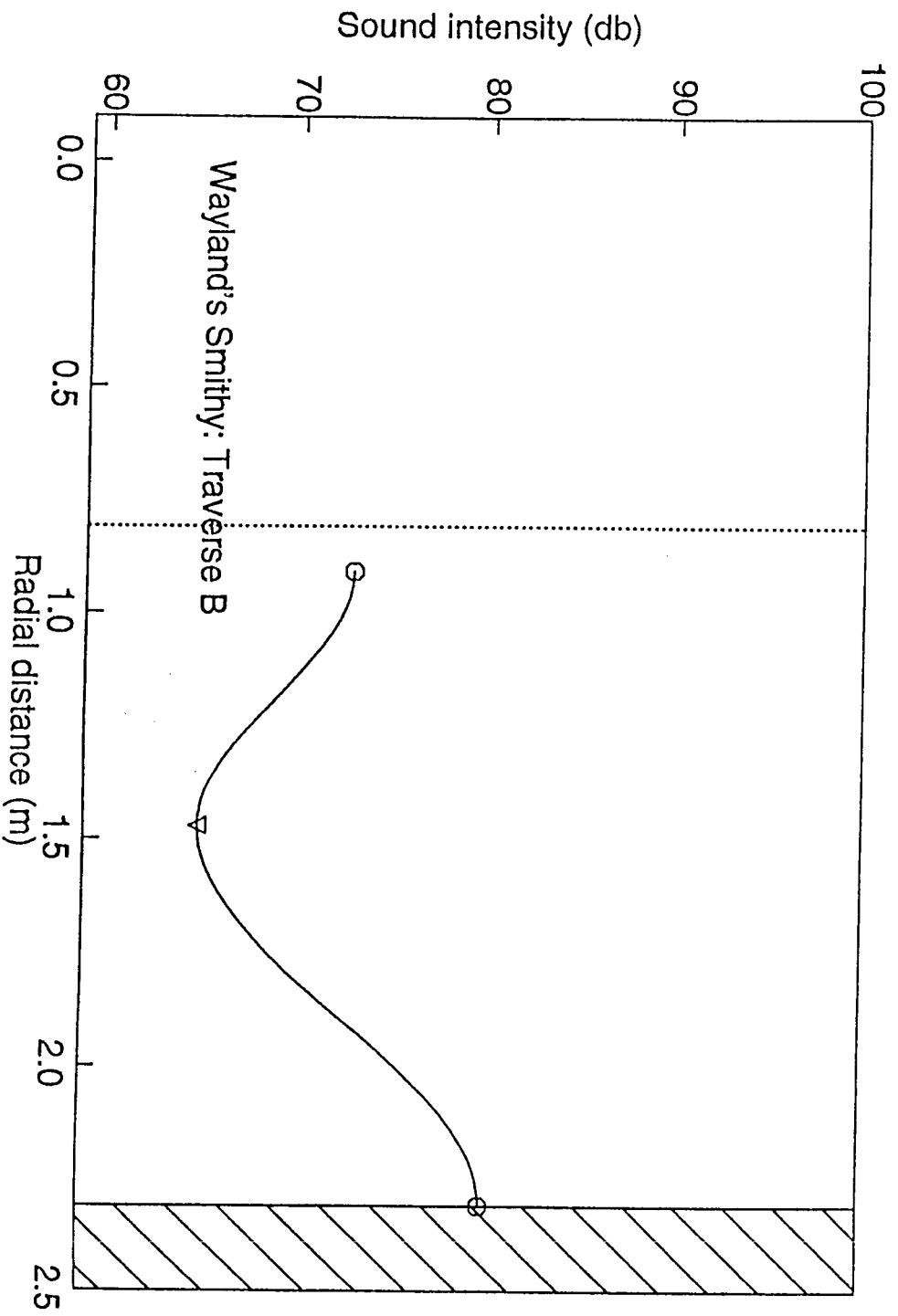
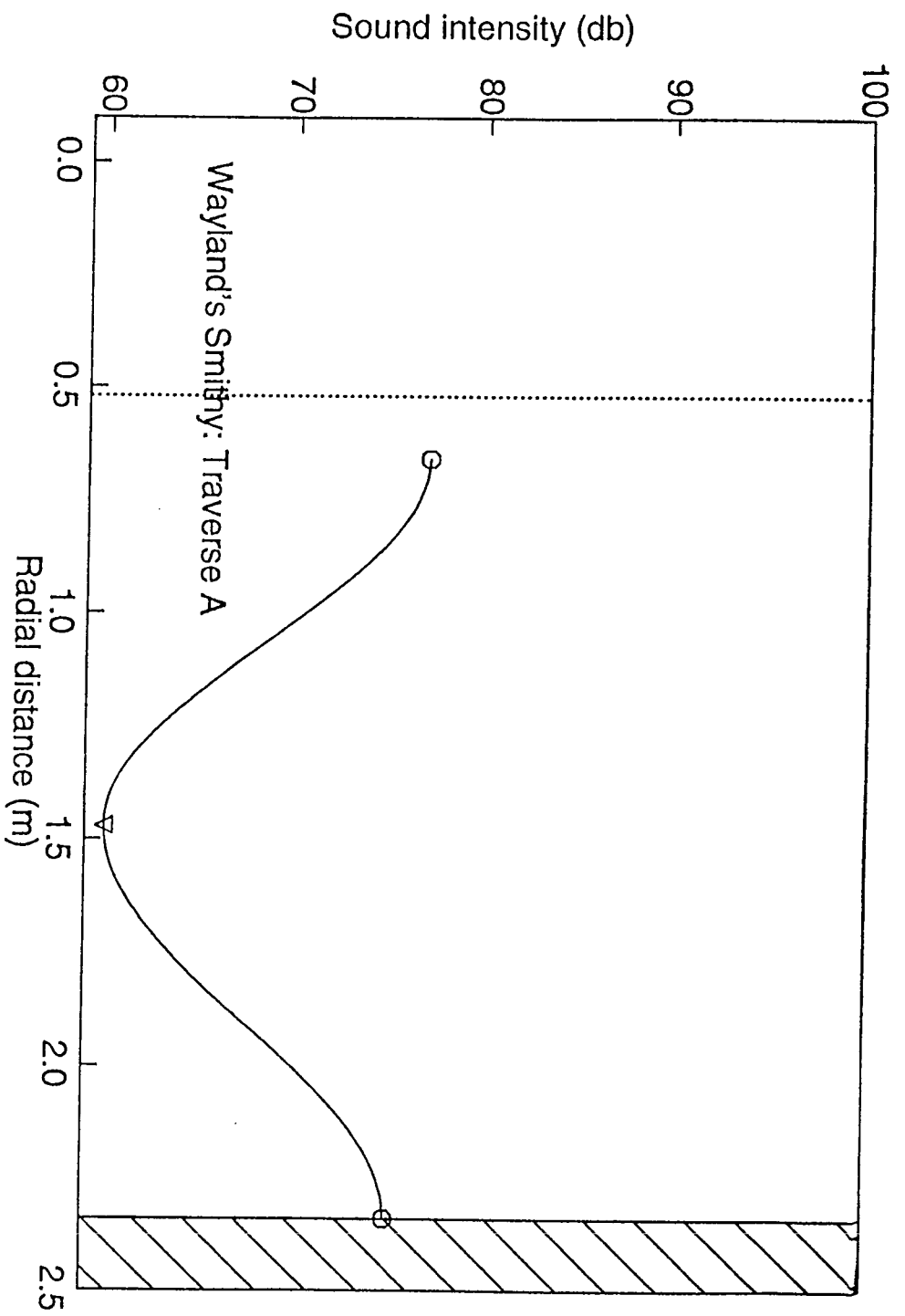


Fig. 1 - Entrance to Wayland's Smithy

WAYLAND'S SMITHY





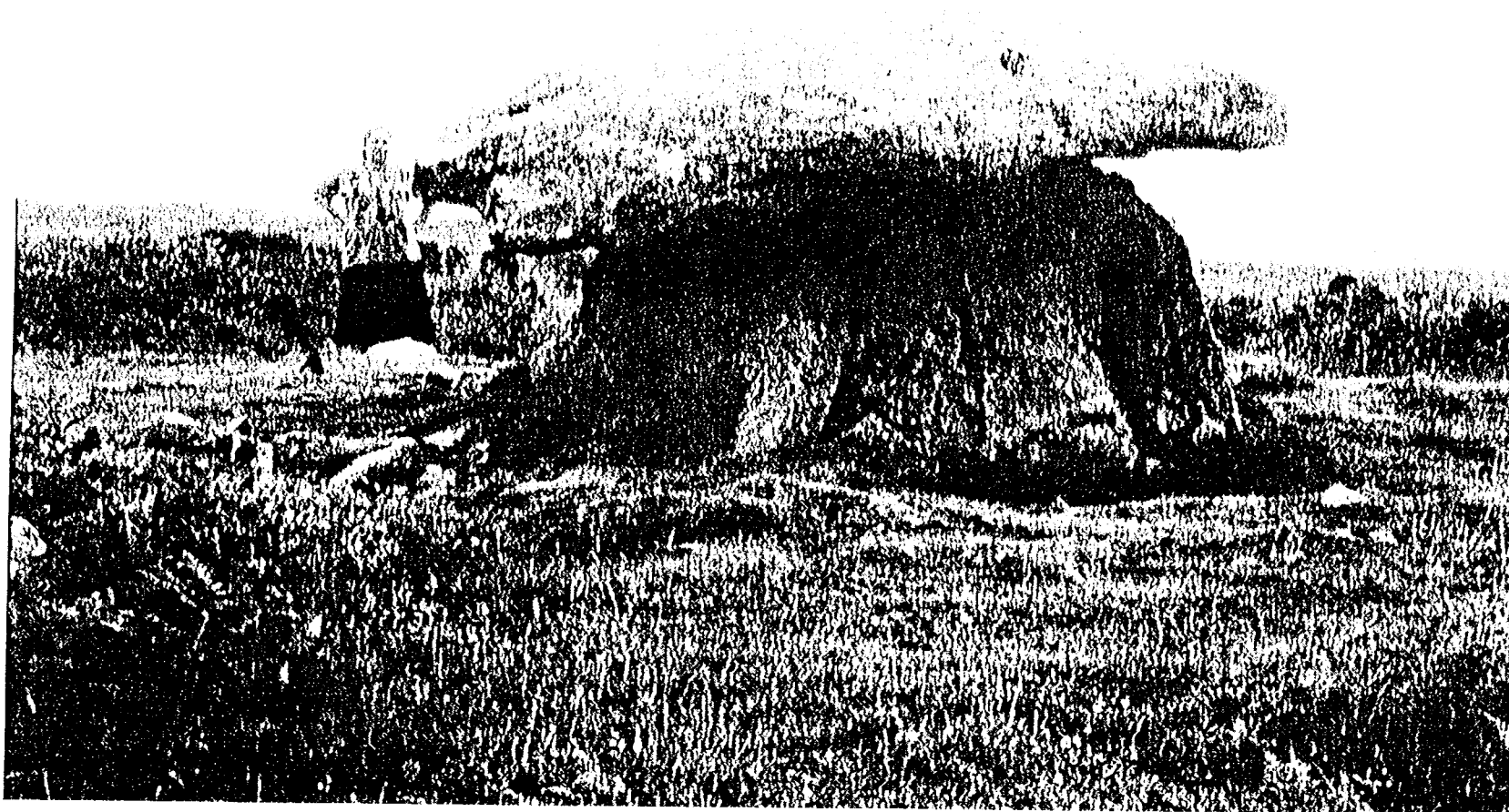
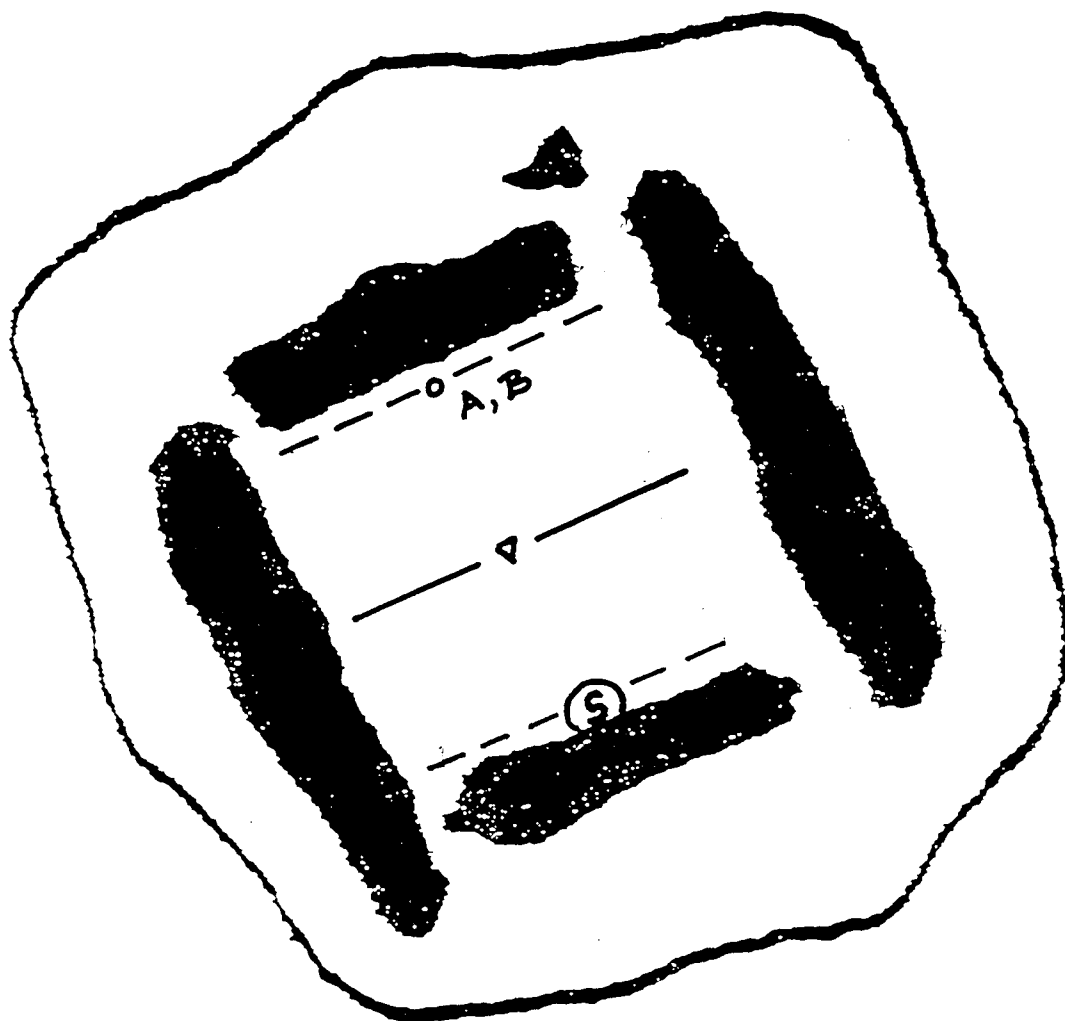


Fig. 2 - Chun Quoit Dolmen

CHUN QUOIT



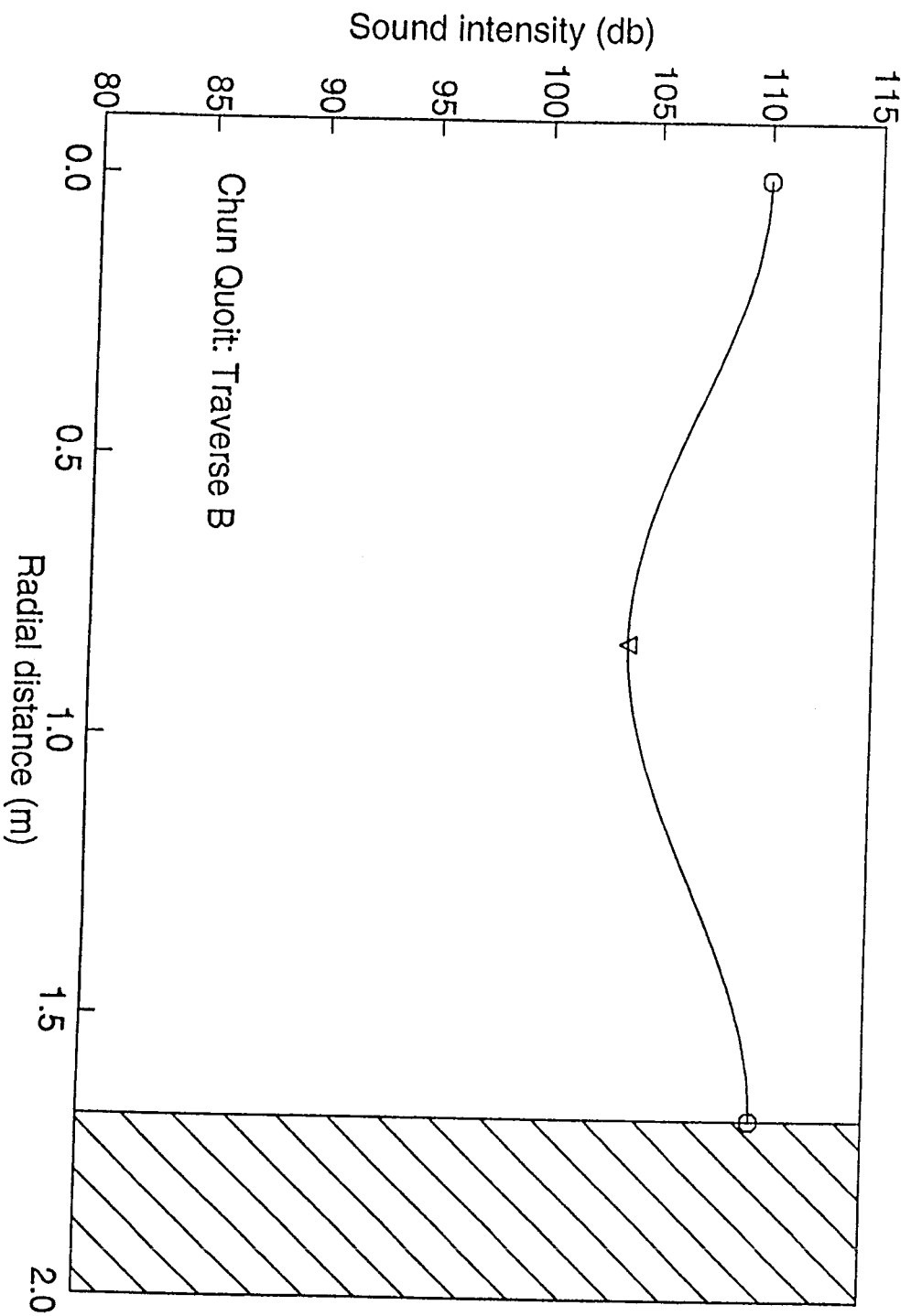
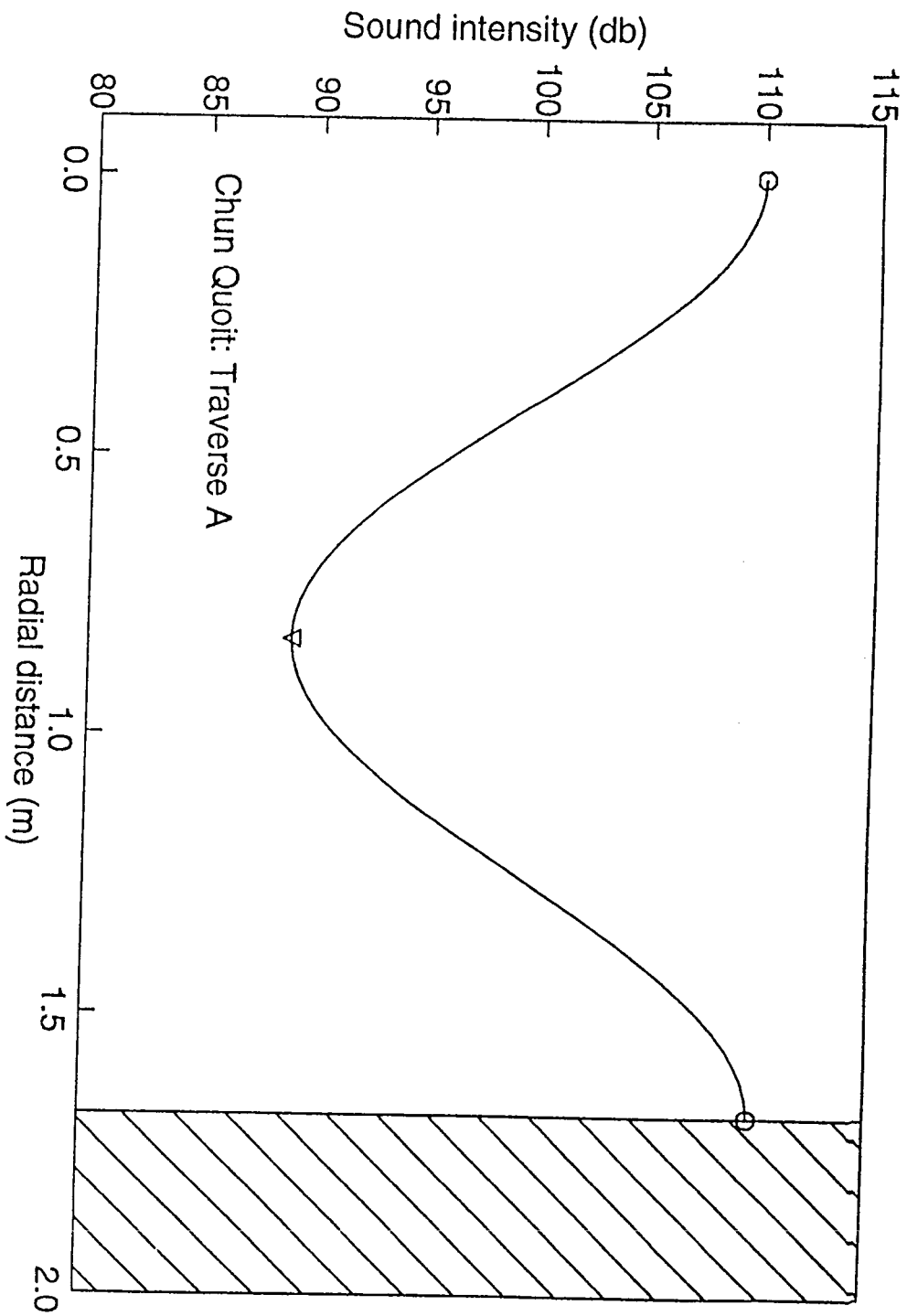
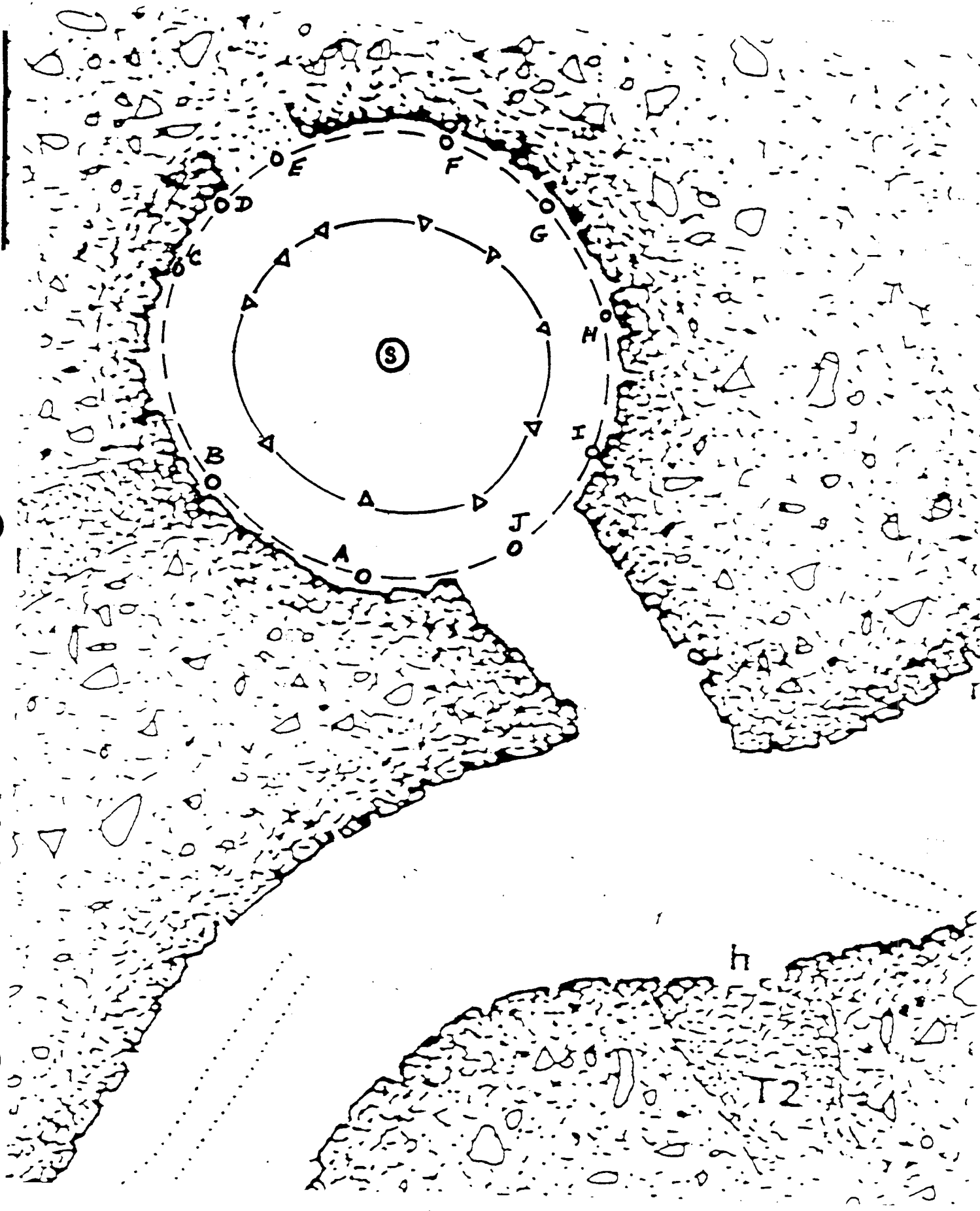
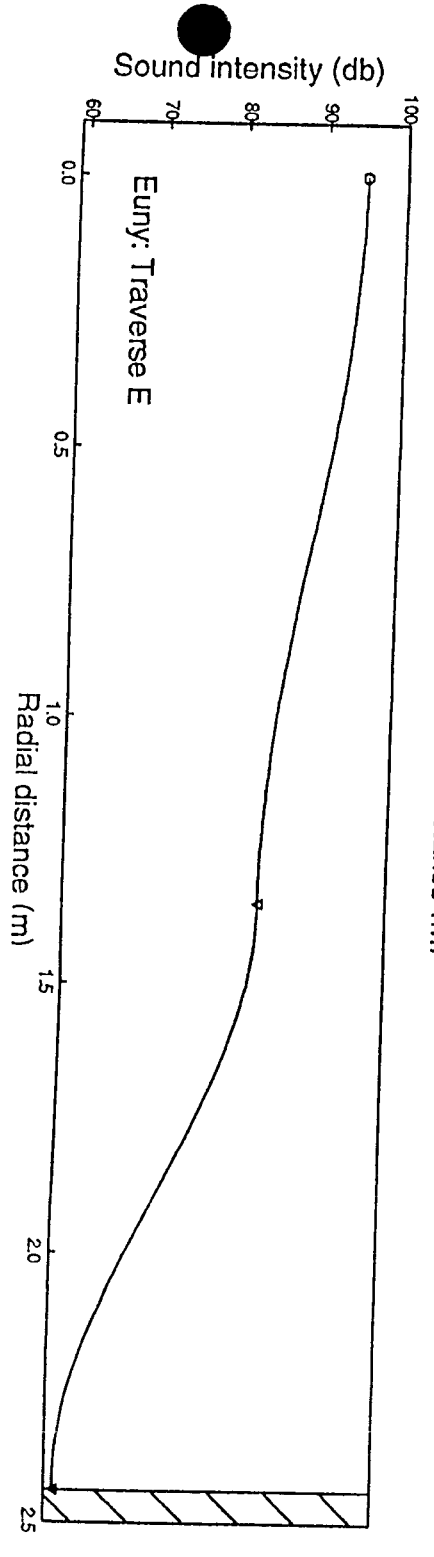
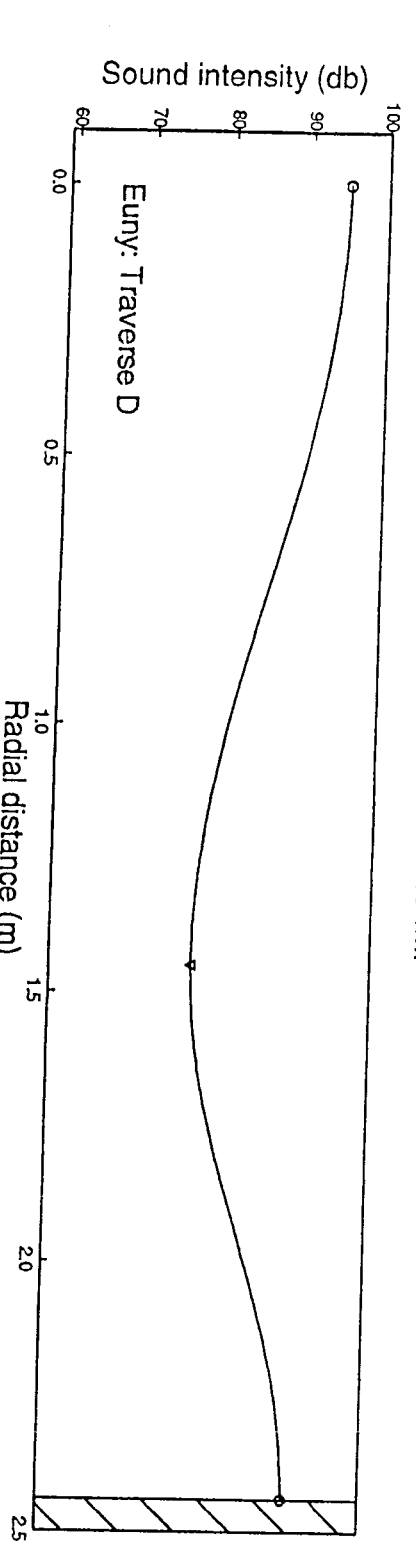
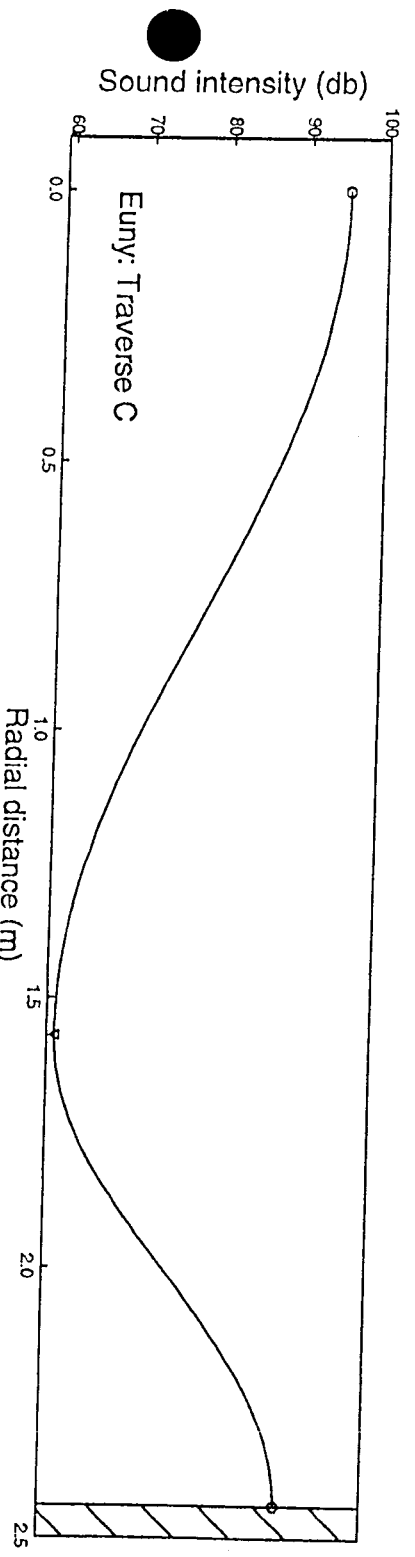
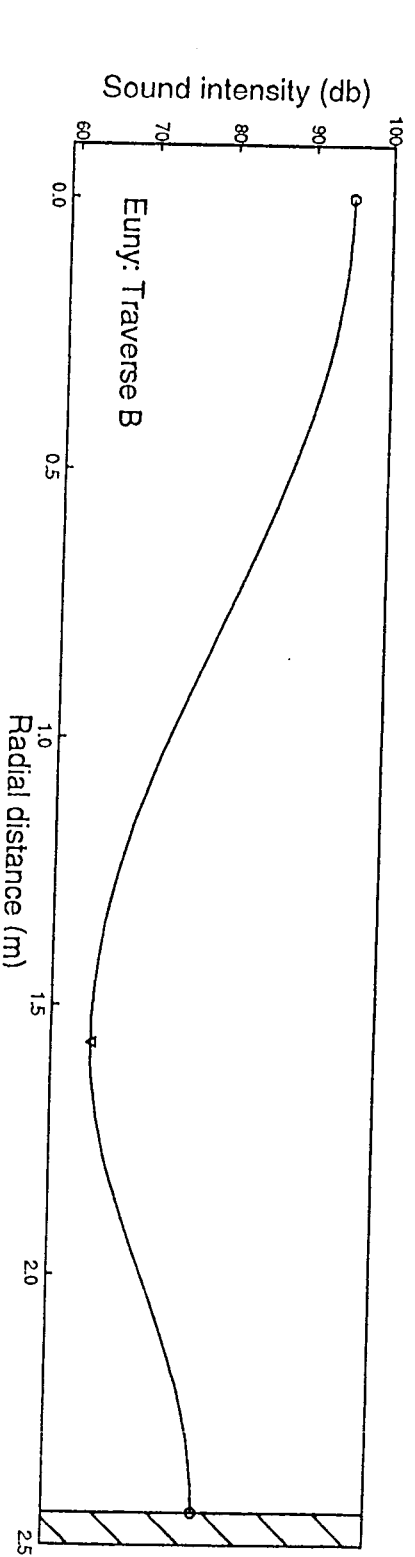
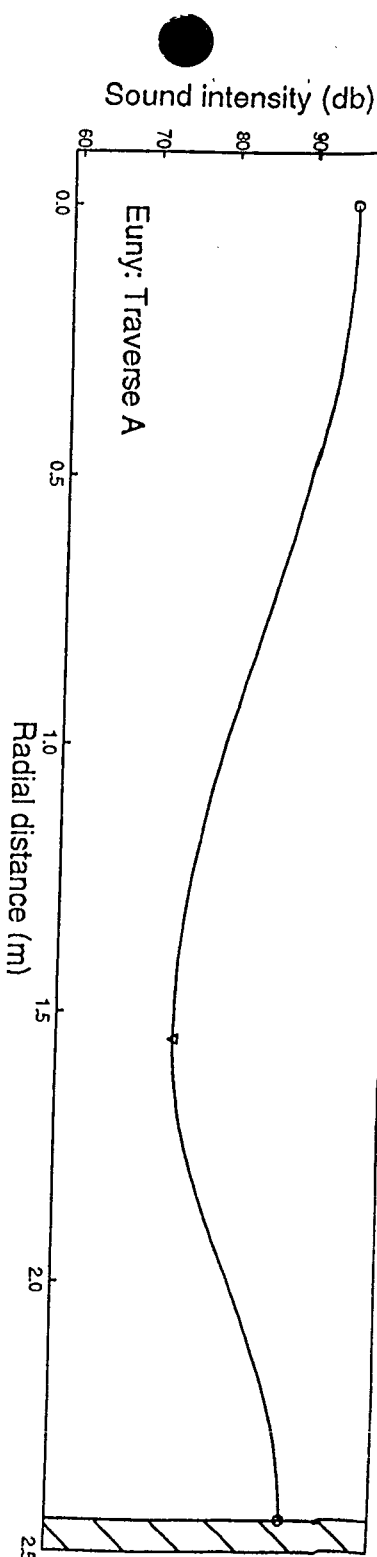


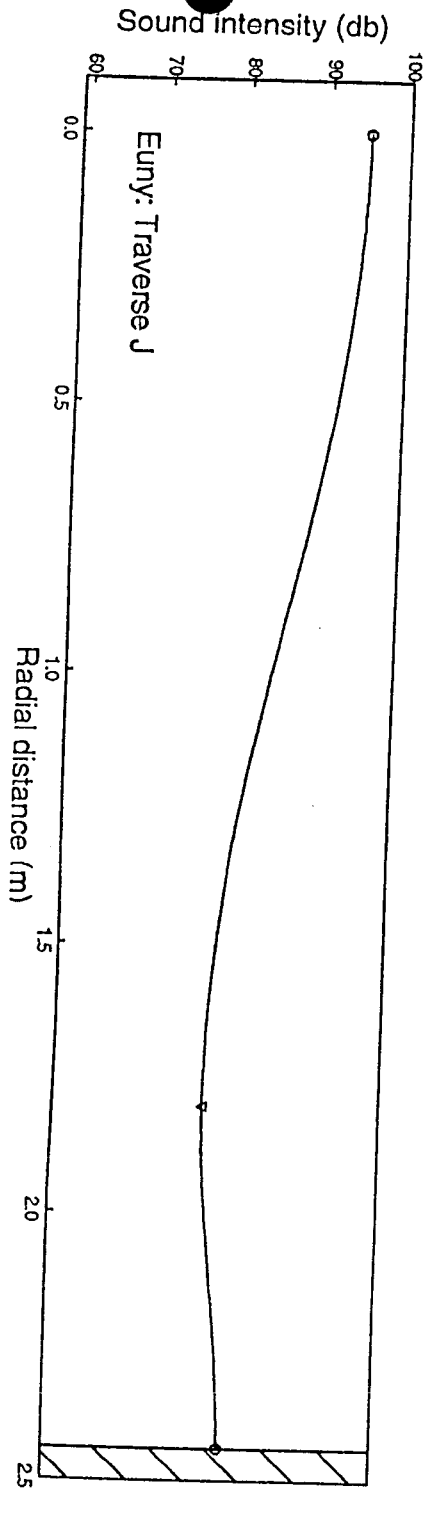
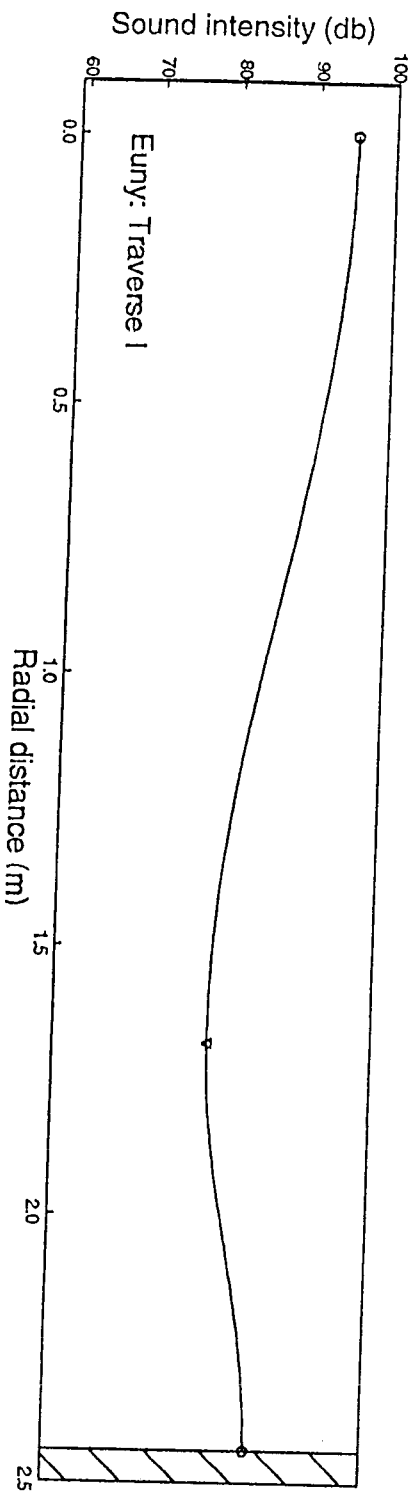
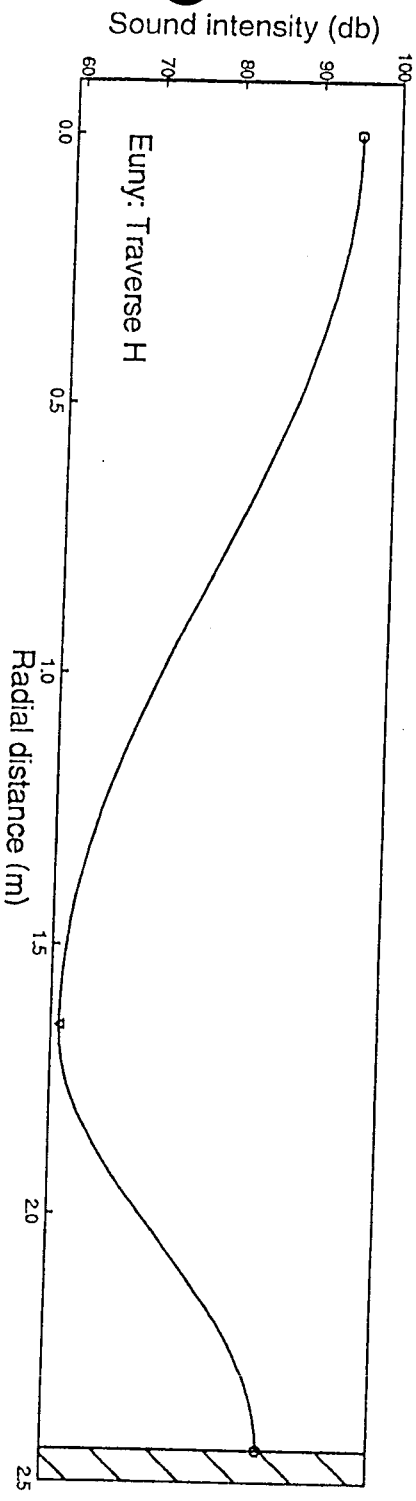
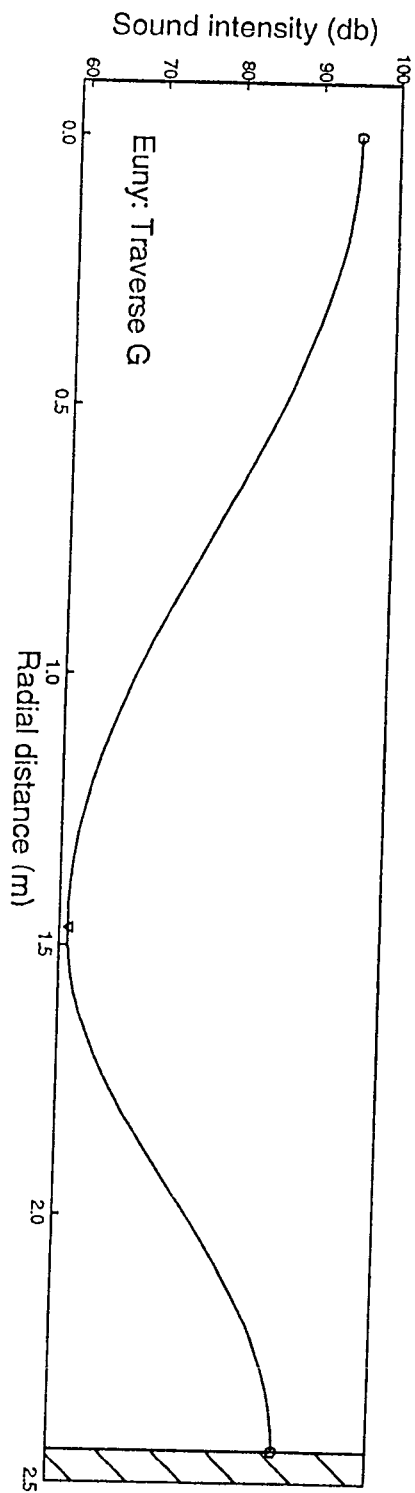
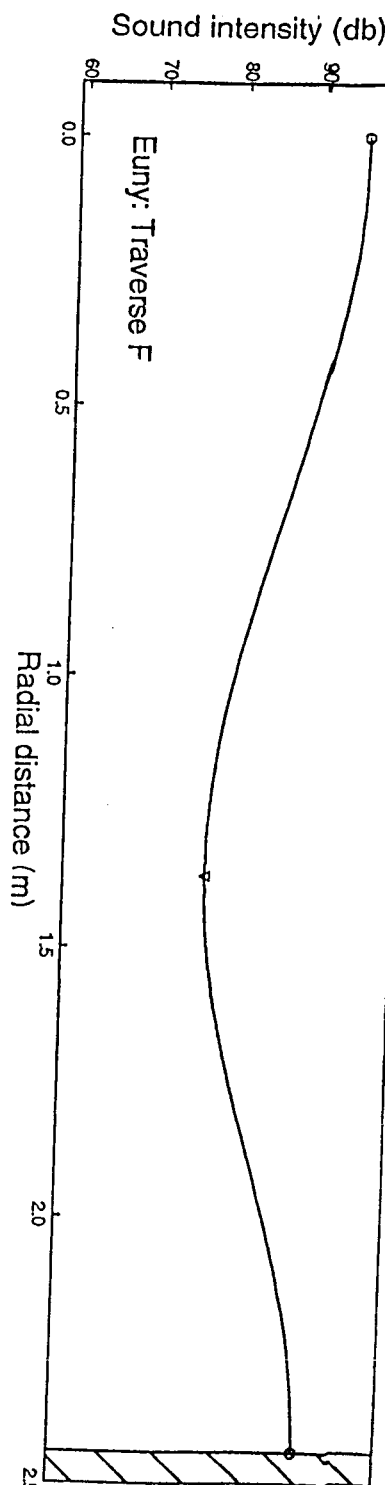


Fig. 3 - Cairn Euny Interior Wall and Recess

CAIRN EUNY







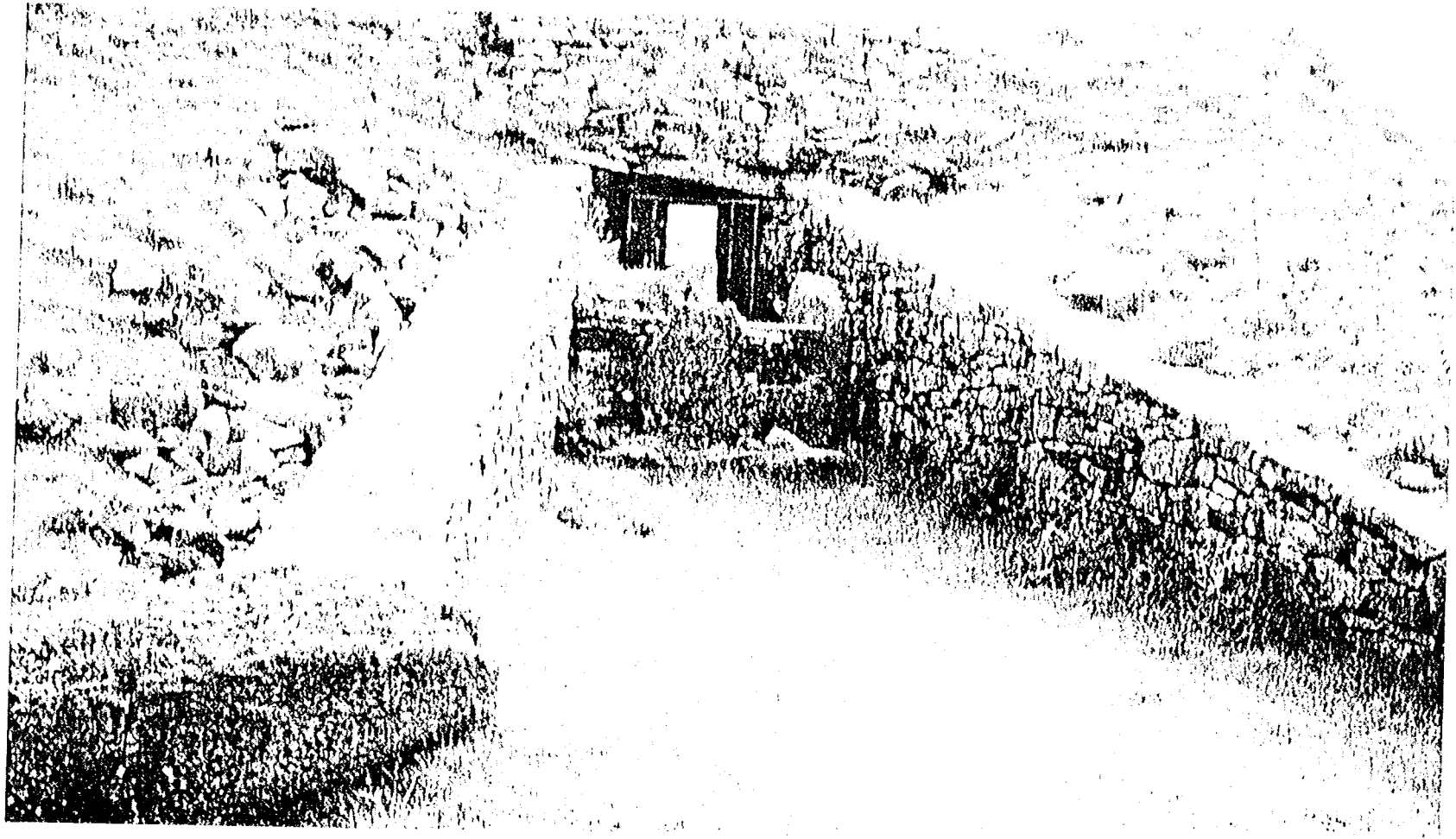
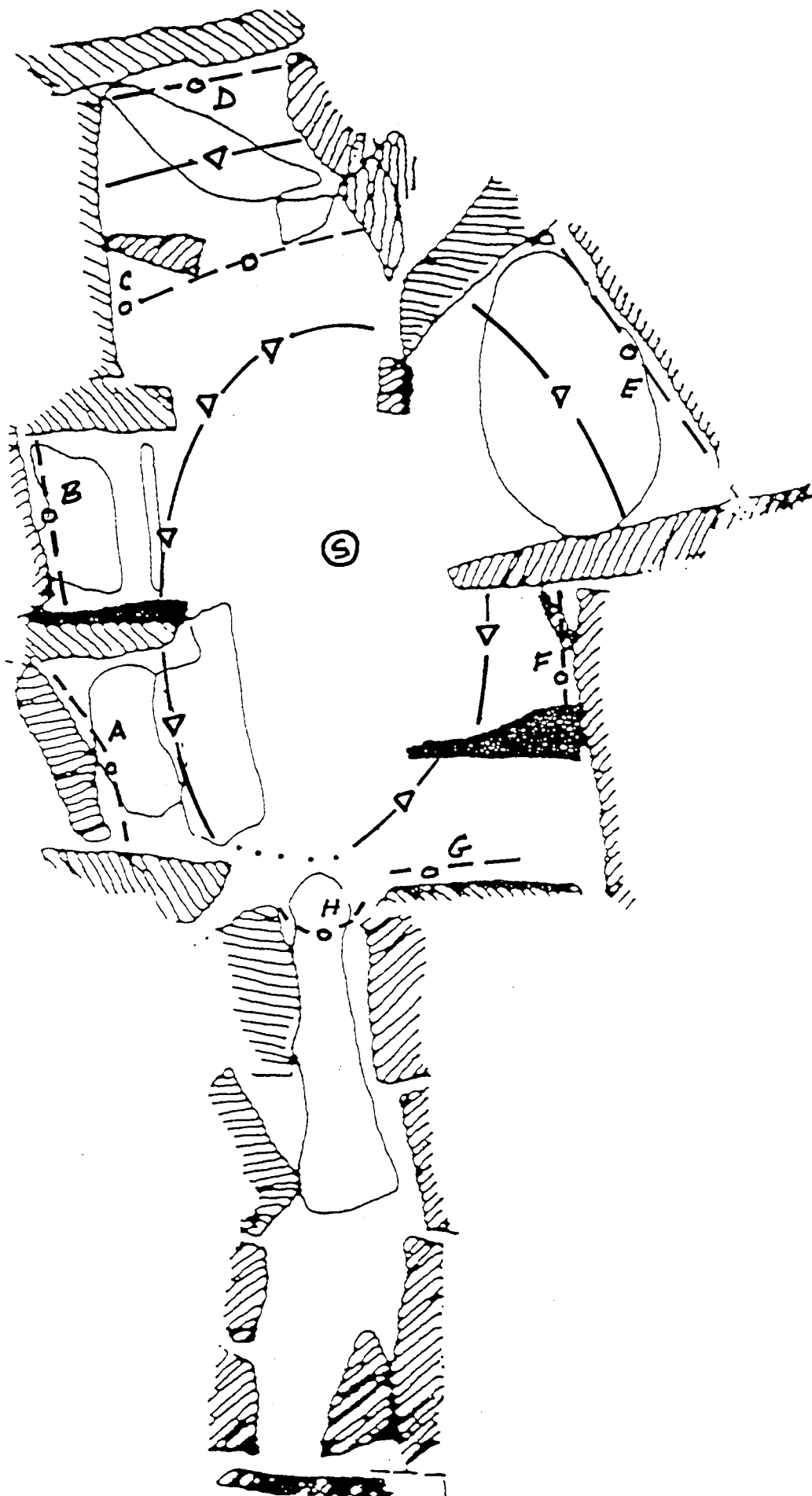
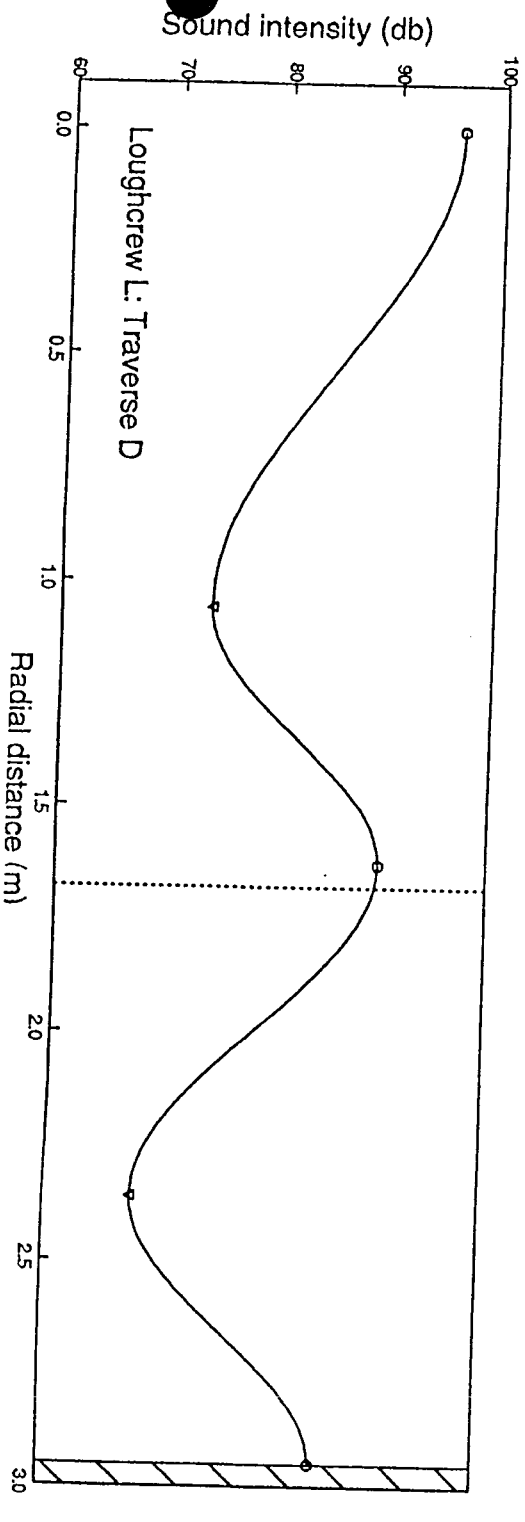
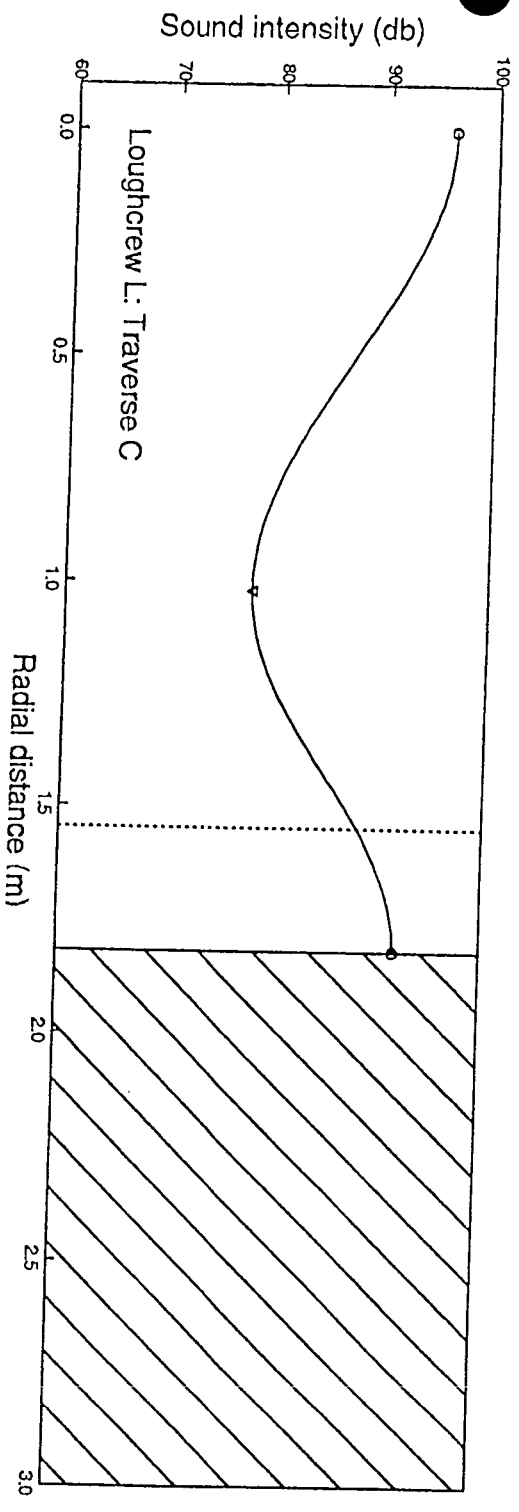
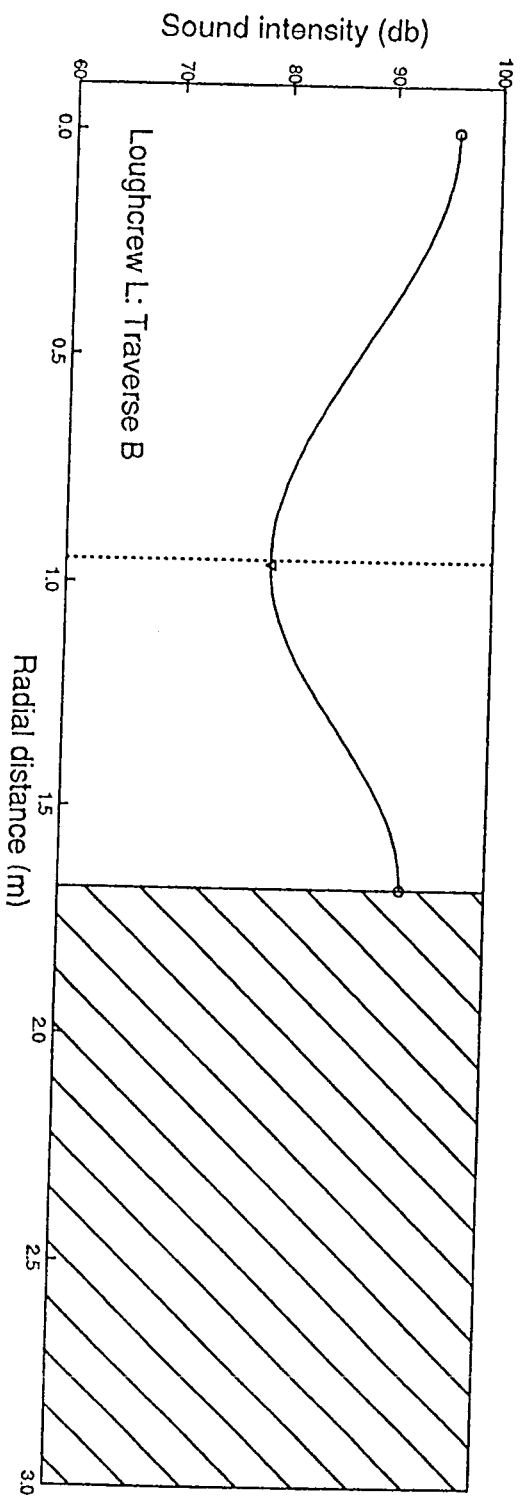
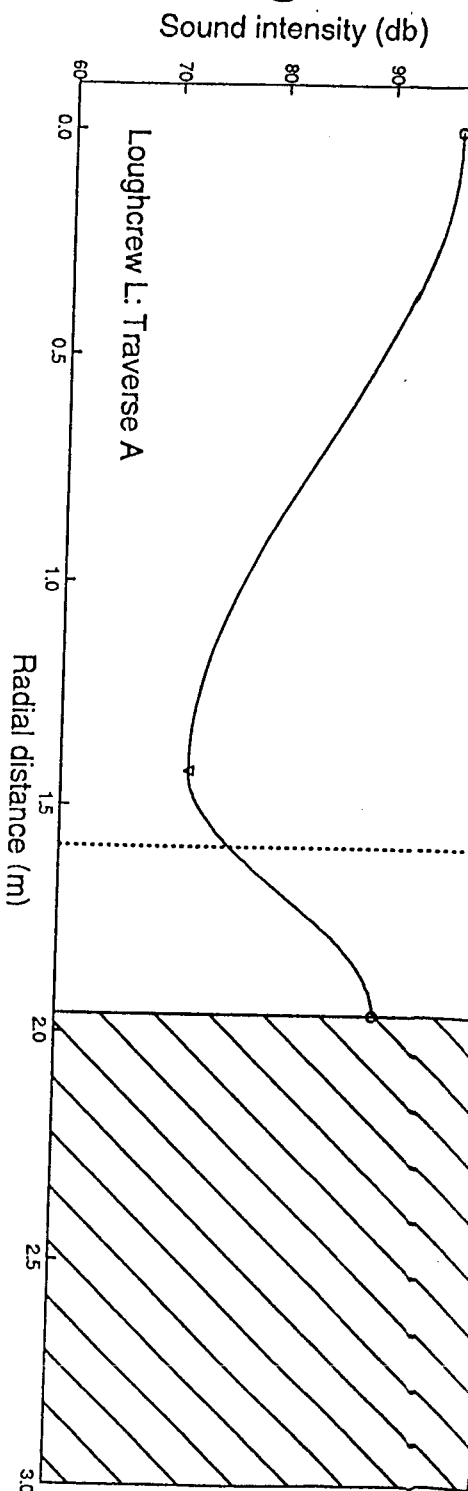
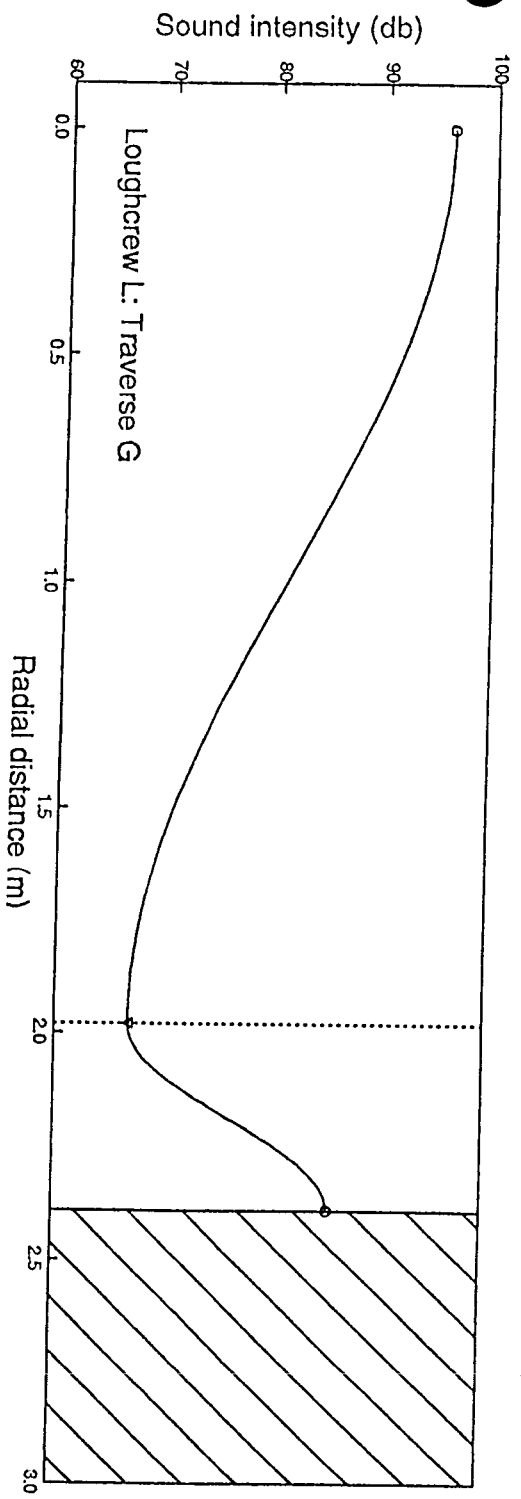
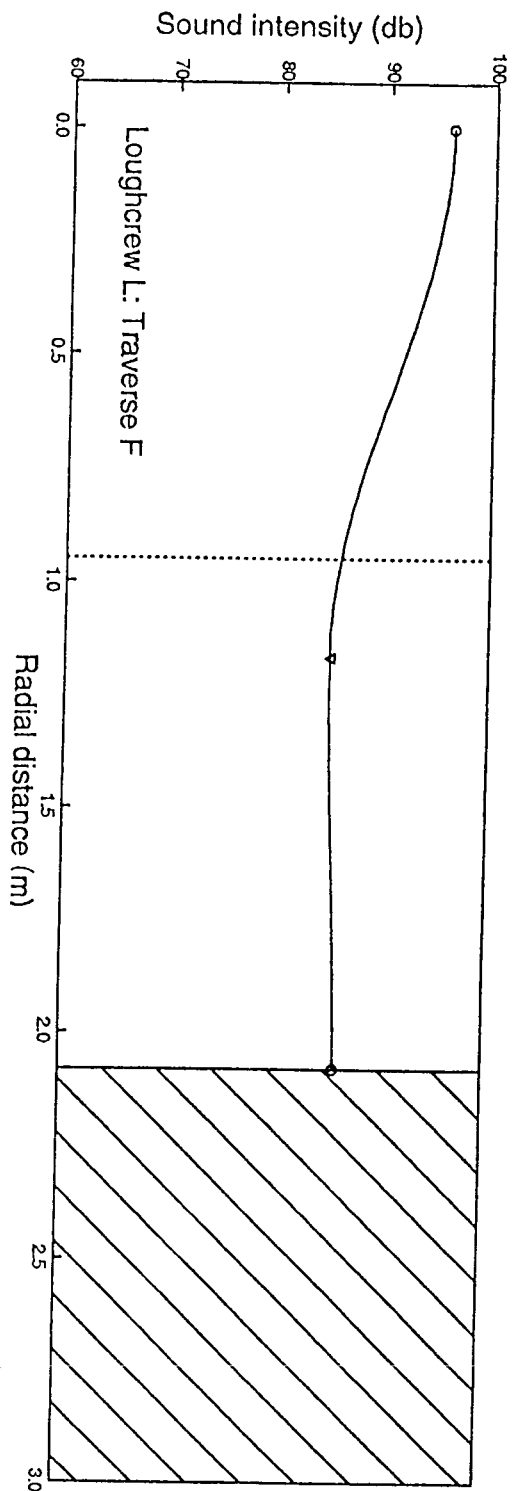
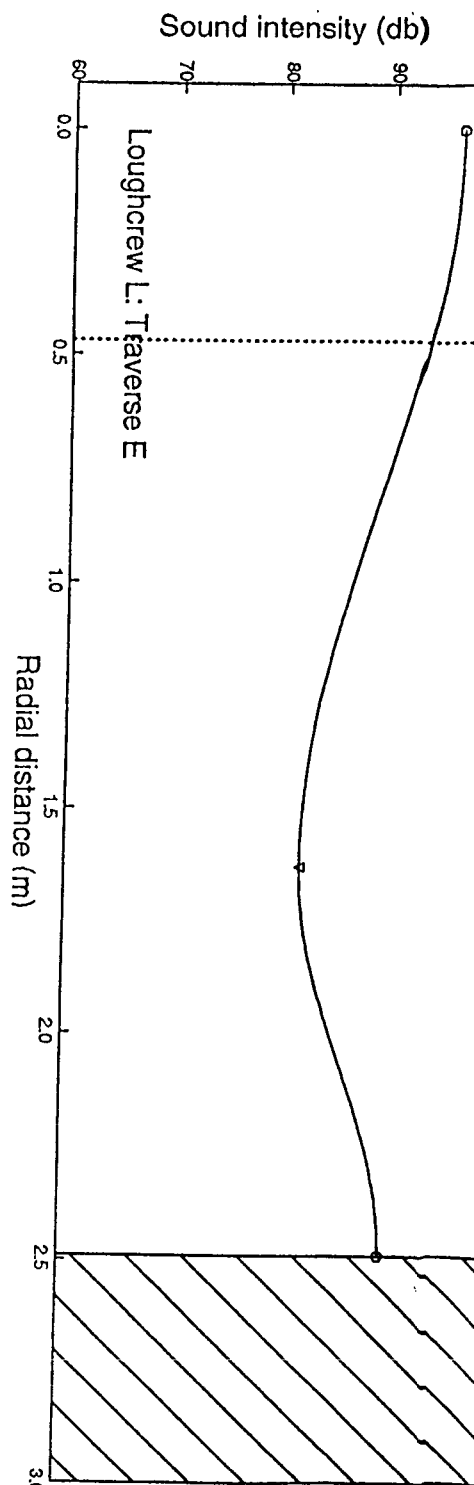


Fig. 4 - Loughcrew Cairn L Entrance Passage

CAIRN L., LOUGHCREW







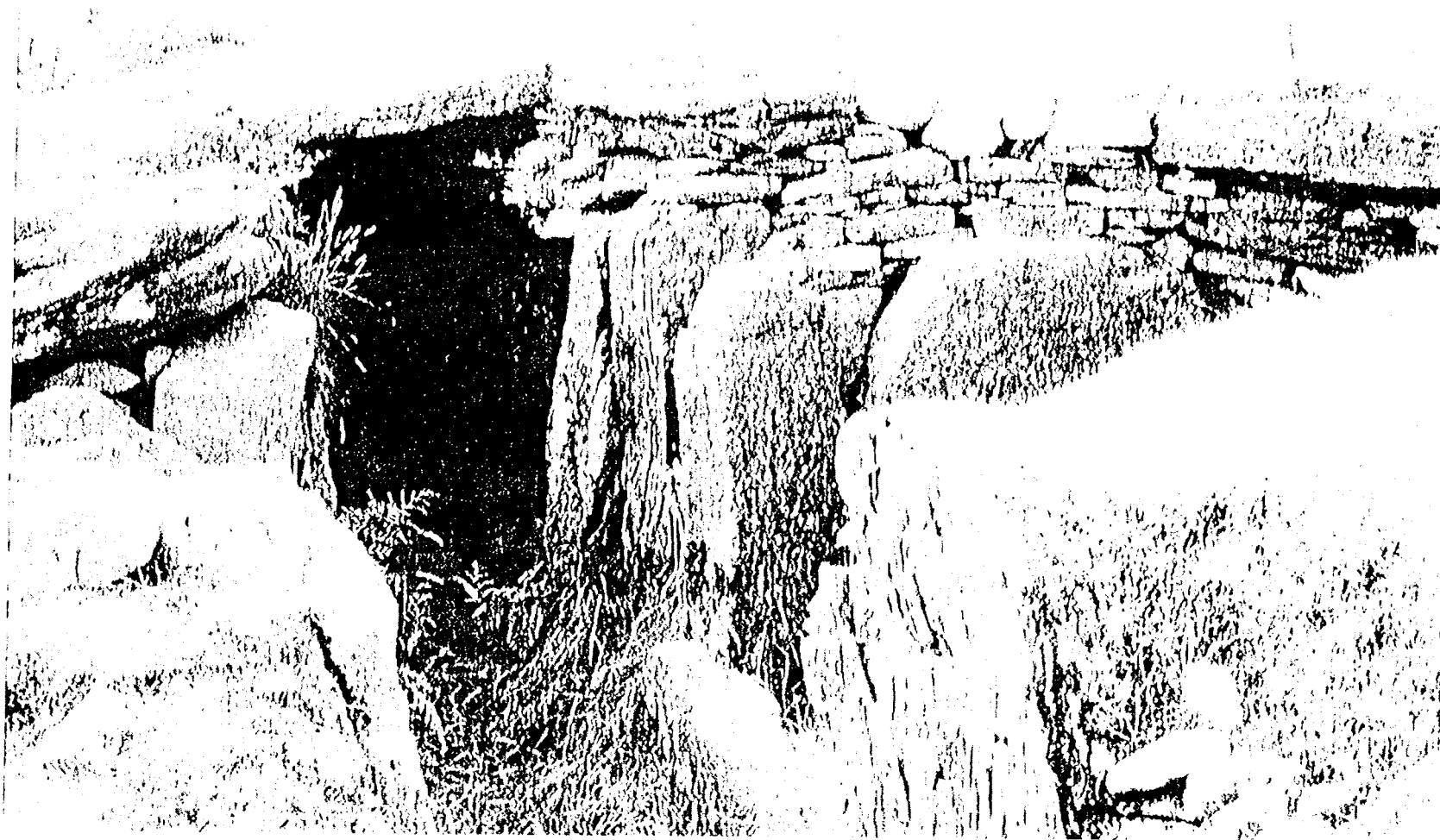
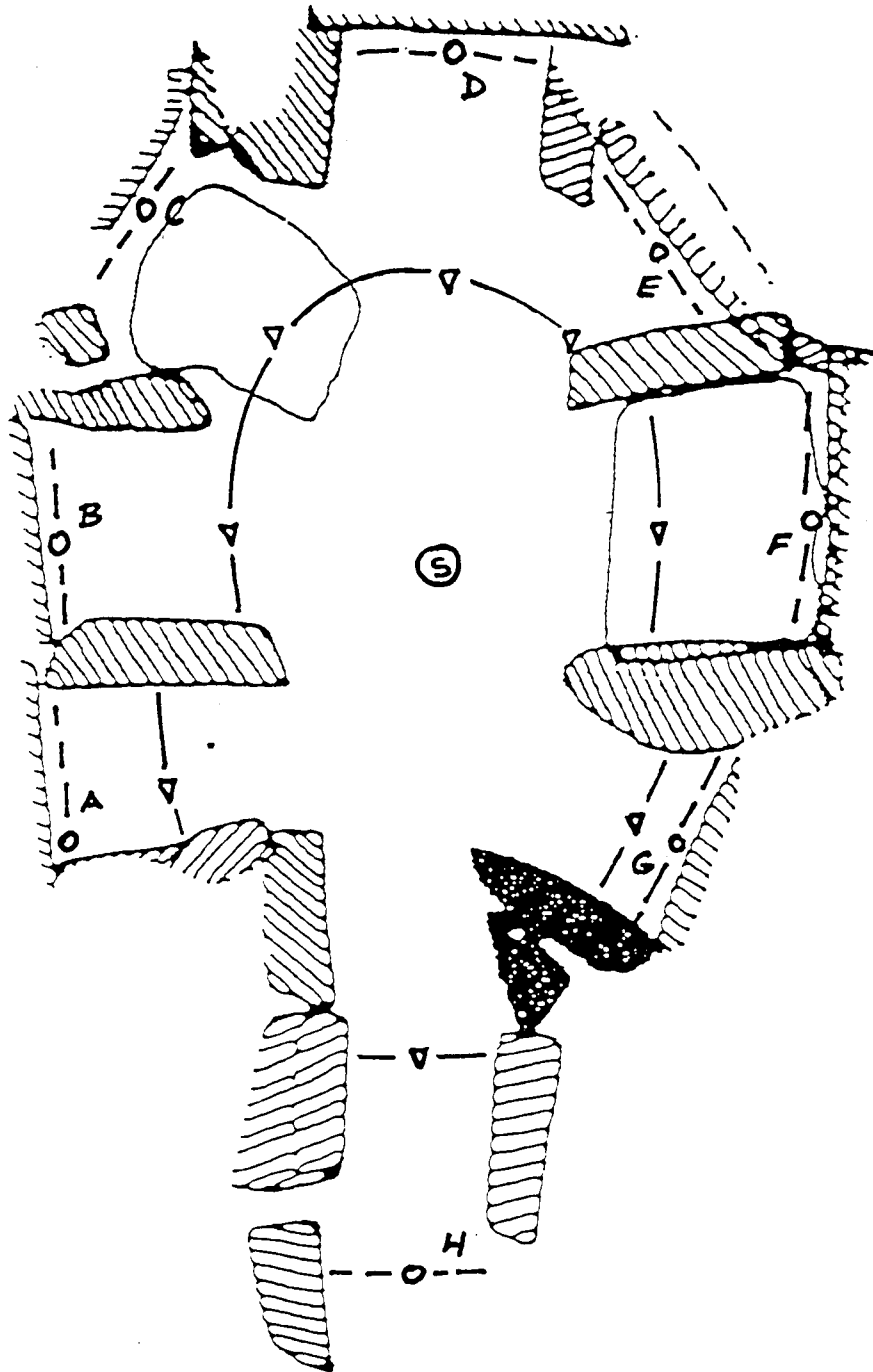
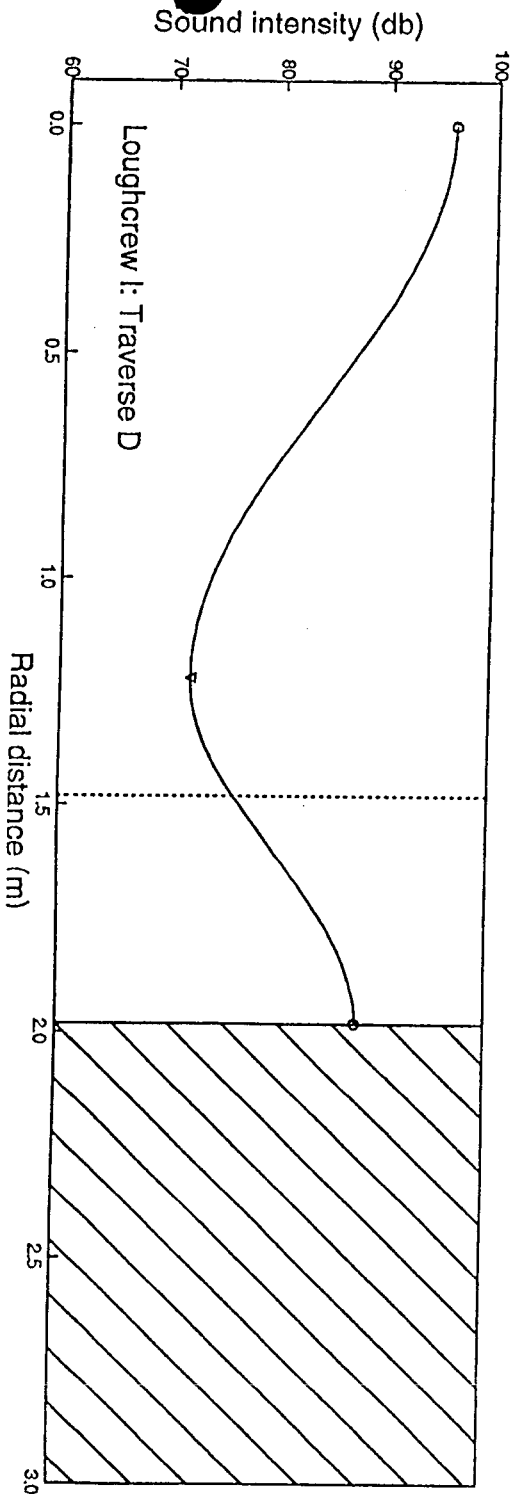
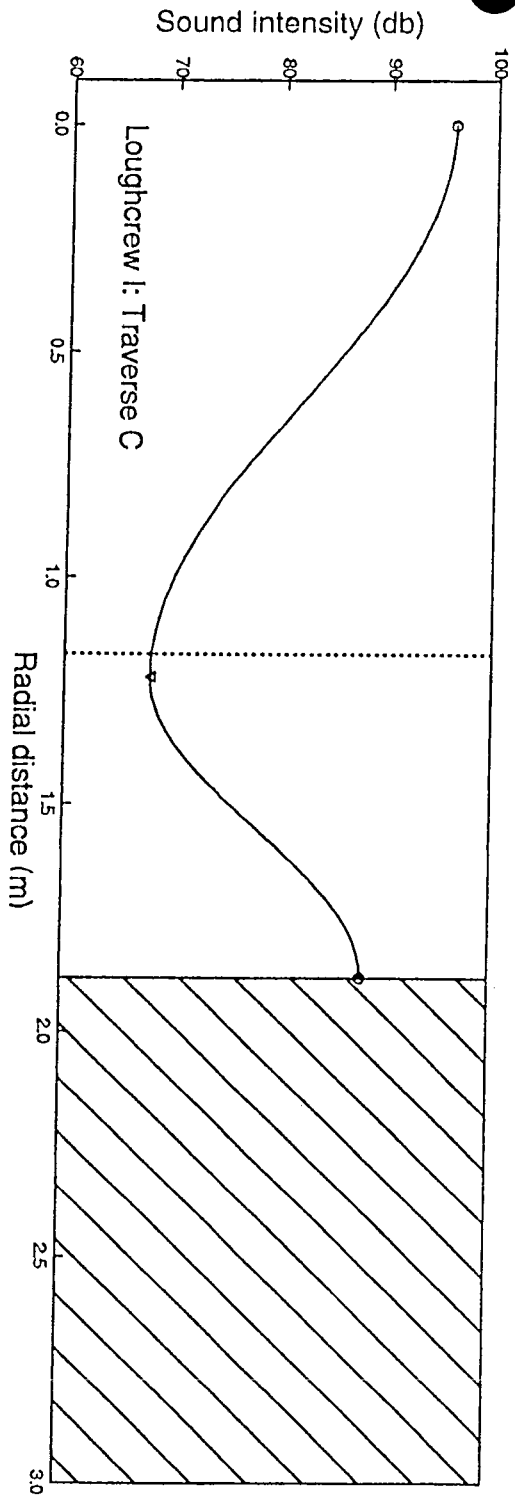
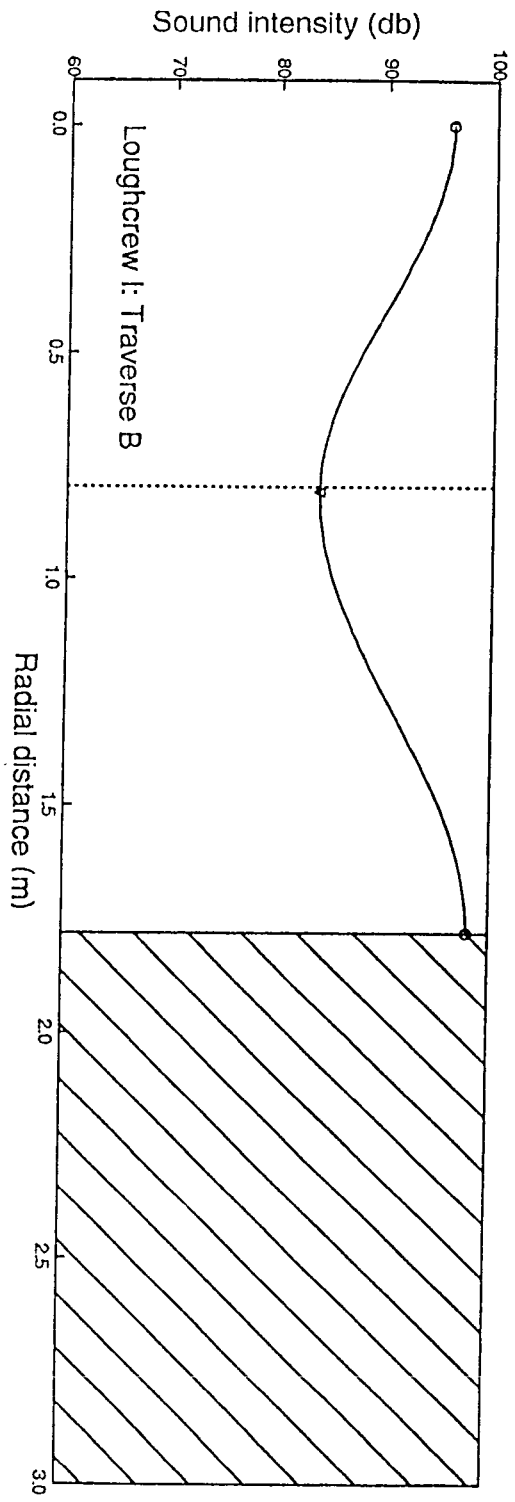
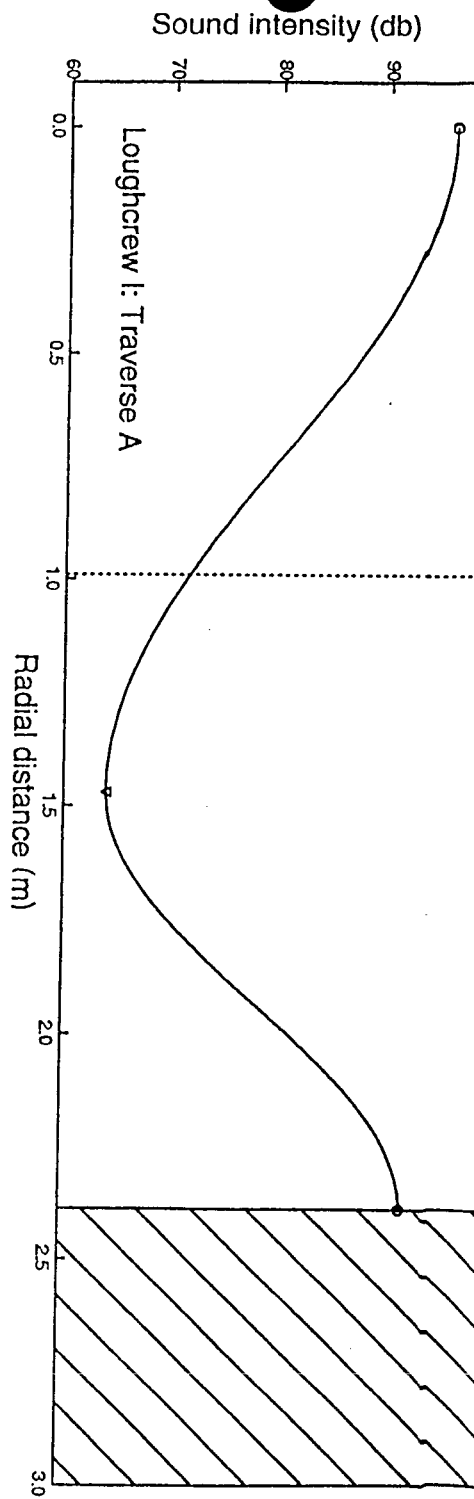


Fig. 5 - Loughcrew Cairn I

CAIRN I





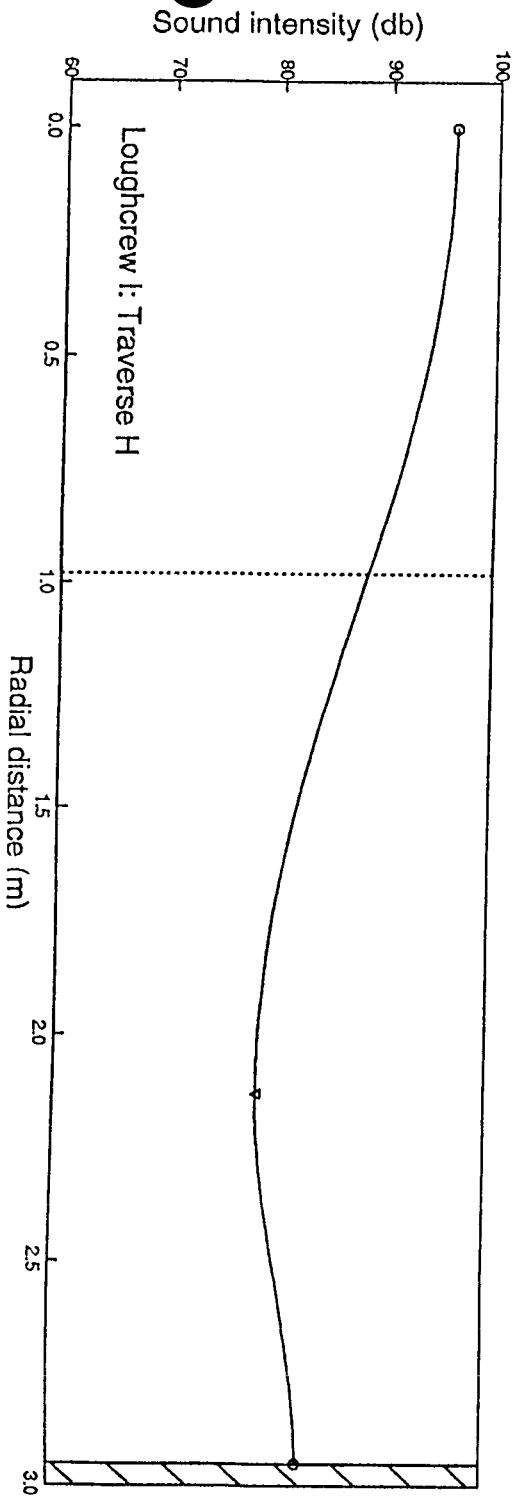
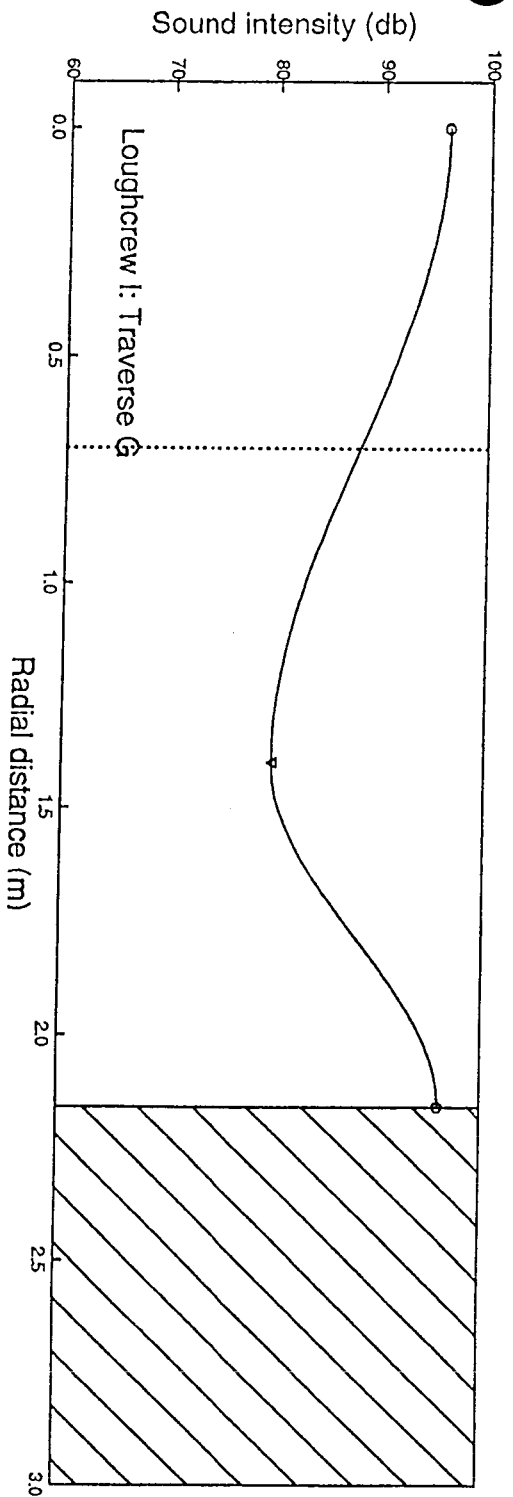
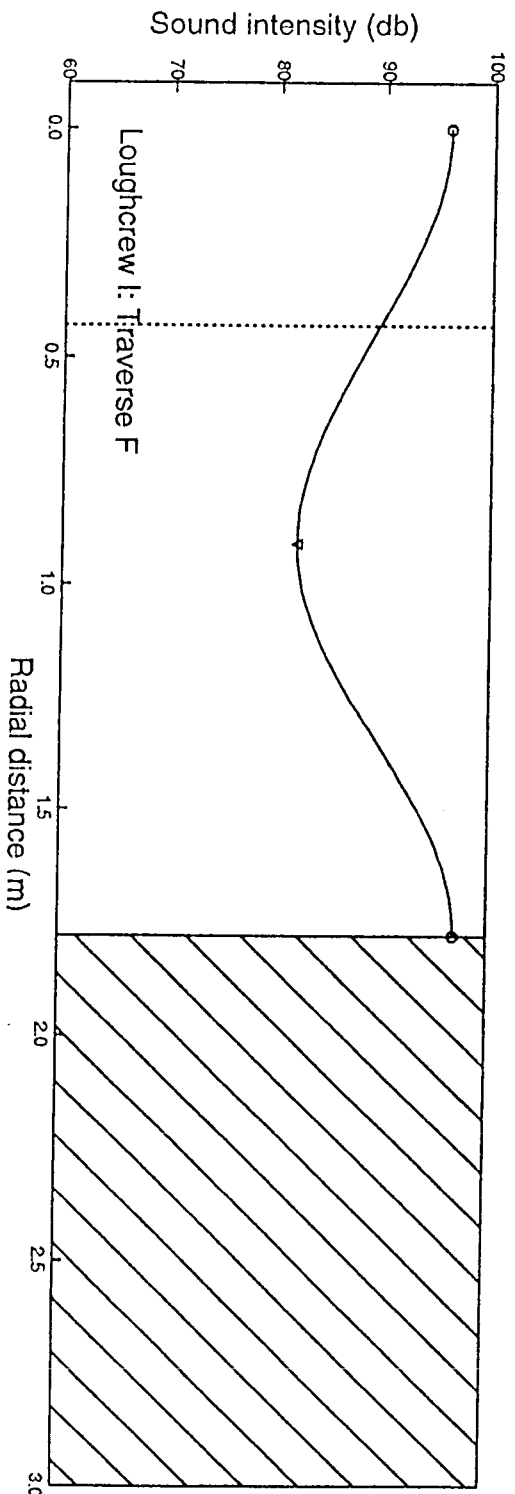
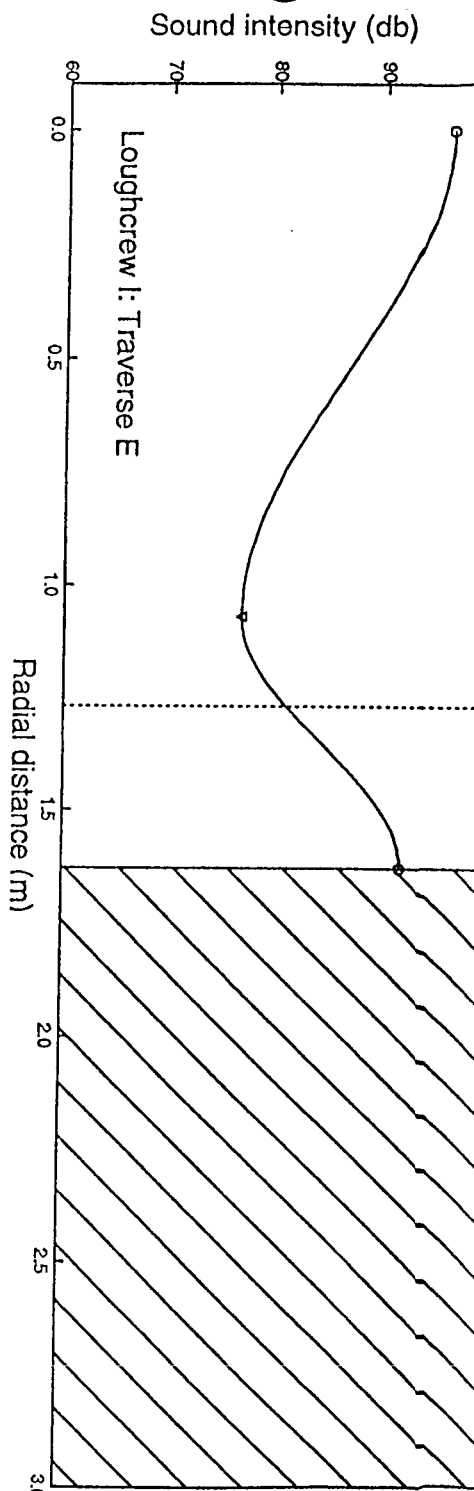
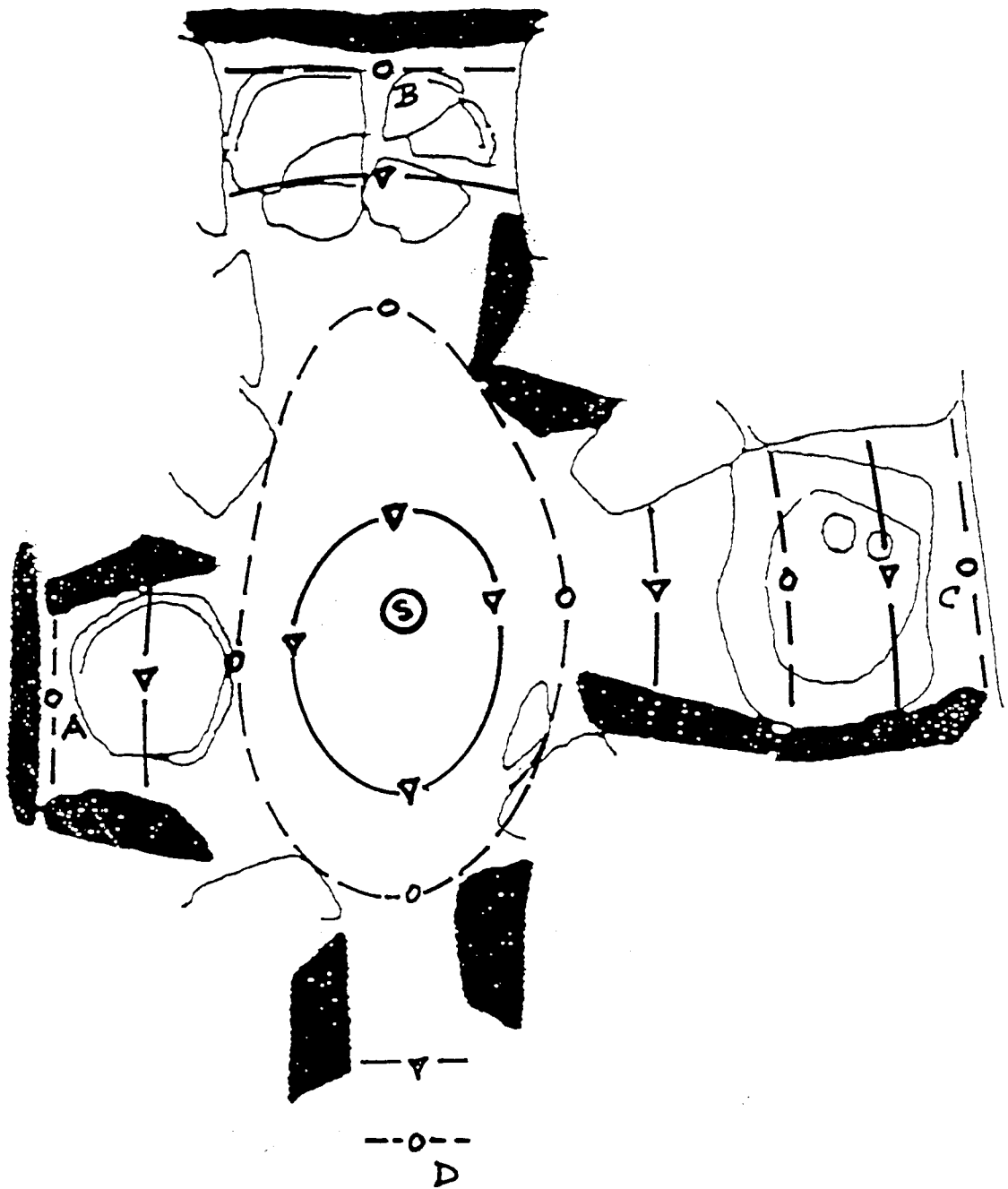
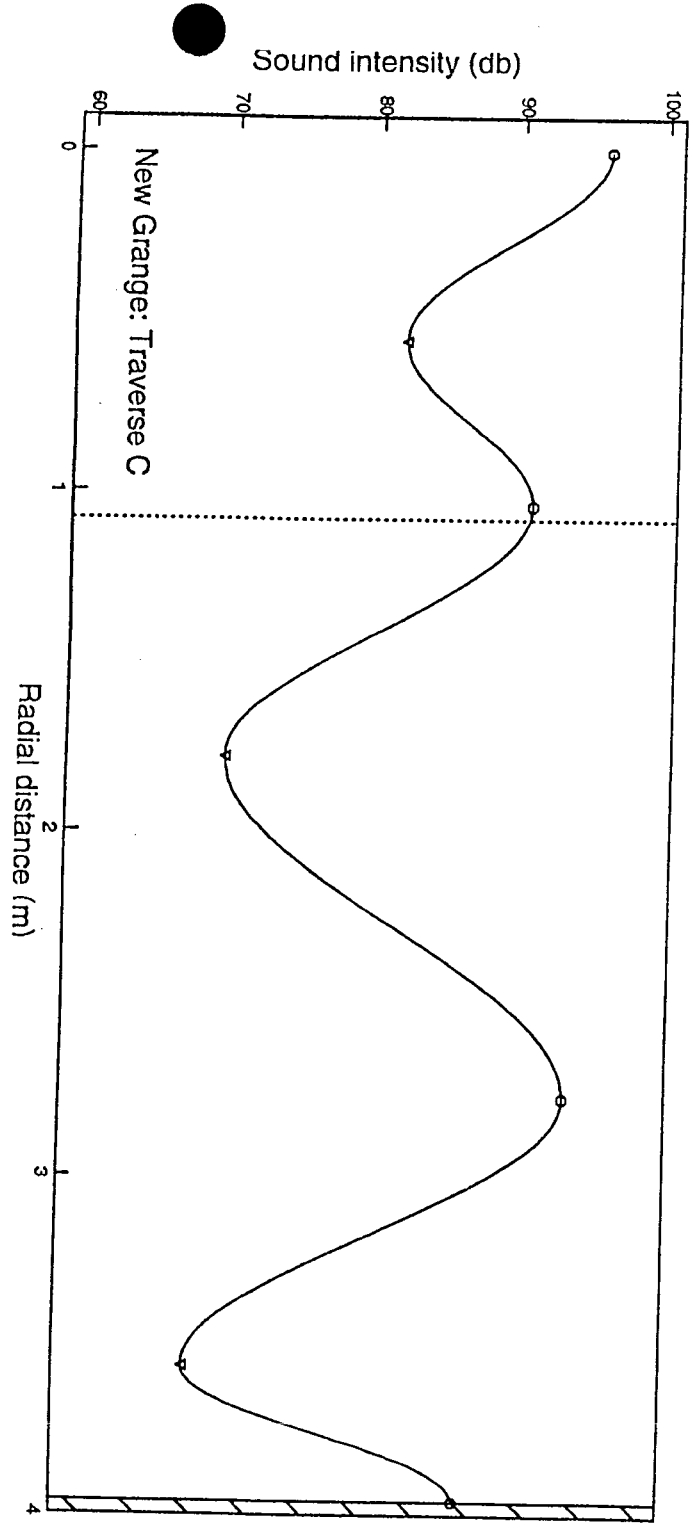
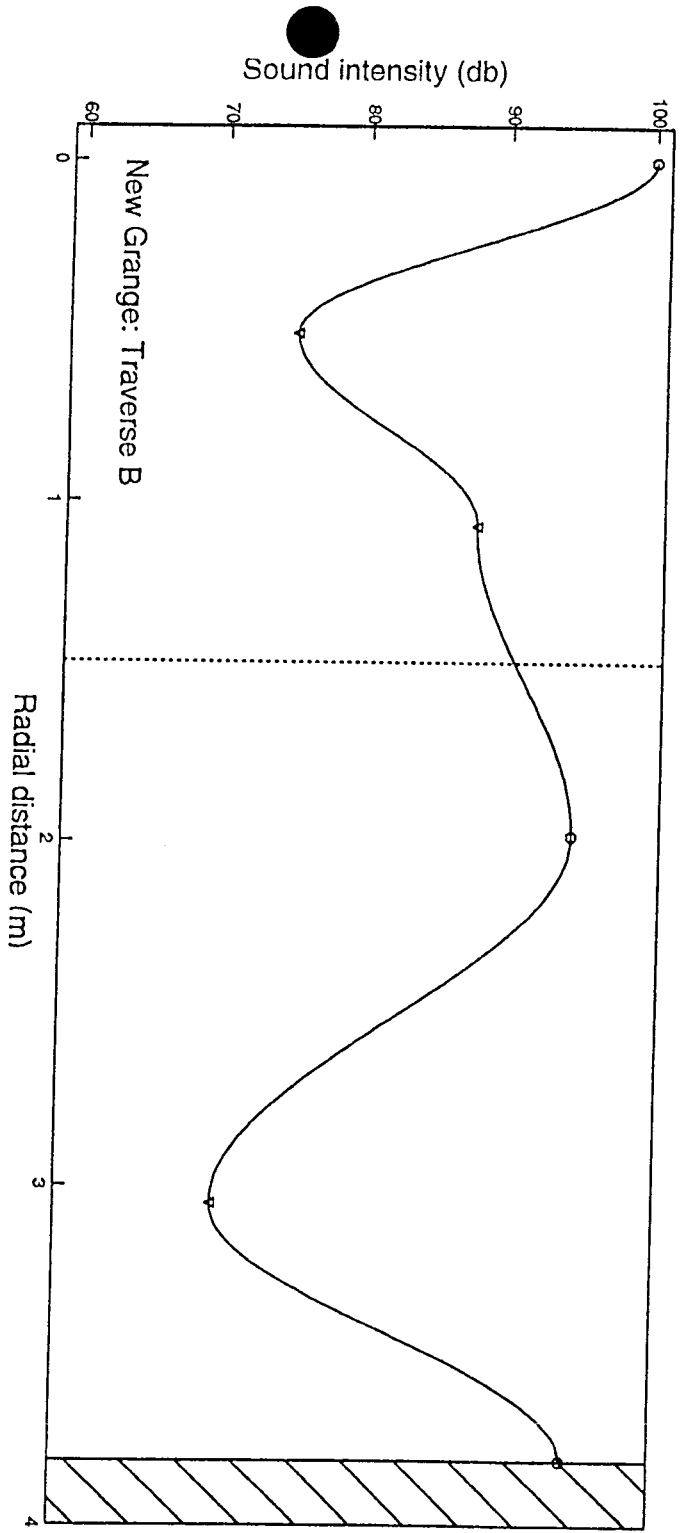
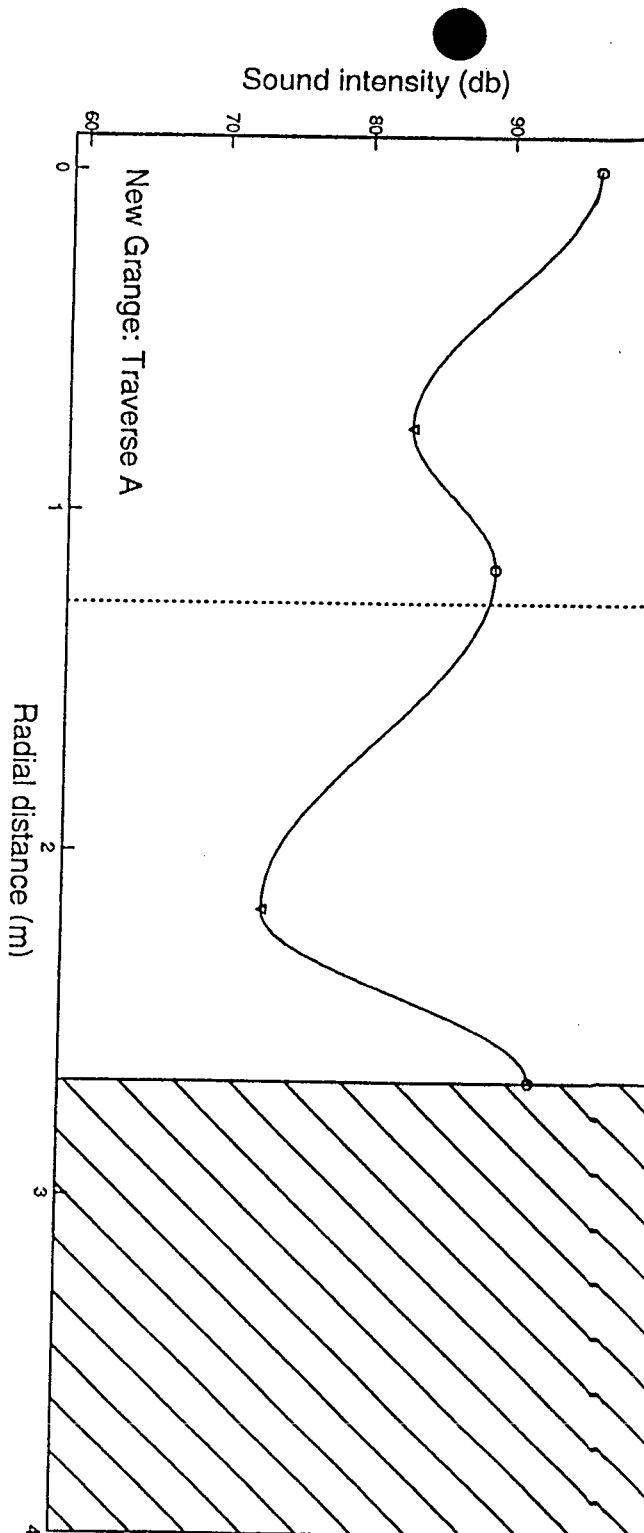




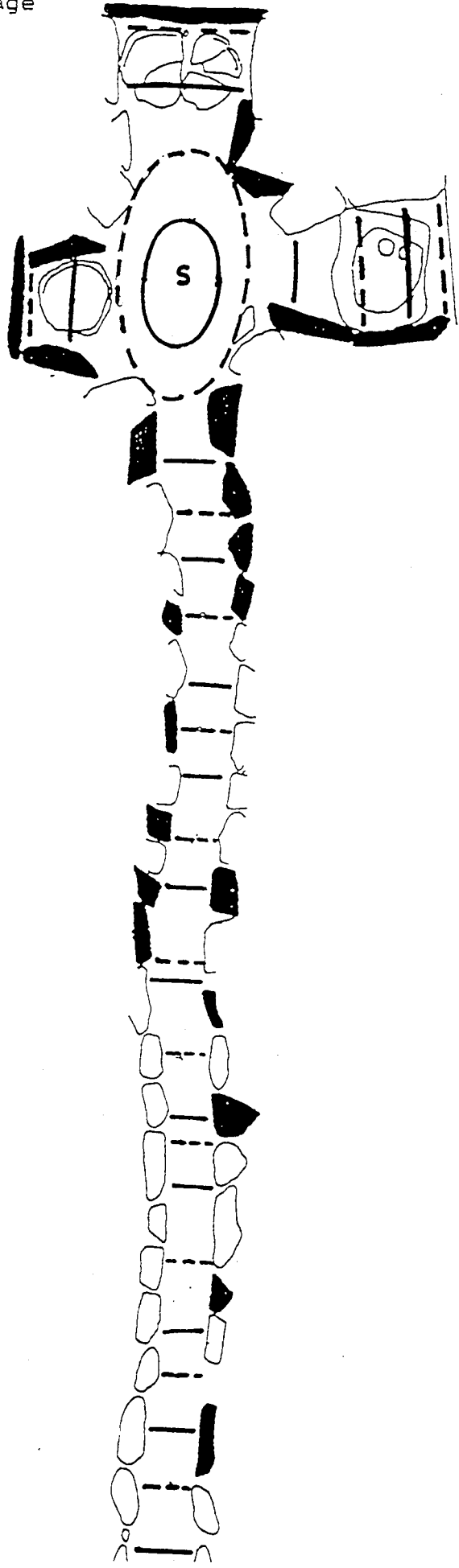
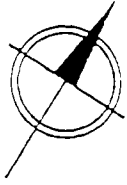
Fig. 6 - Newgrange Exterior

NEWGRANGE  
Chamber





NEWGRANGE  
Passage



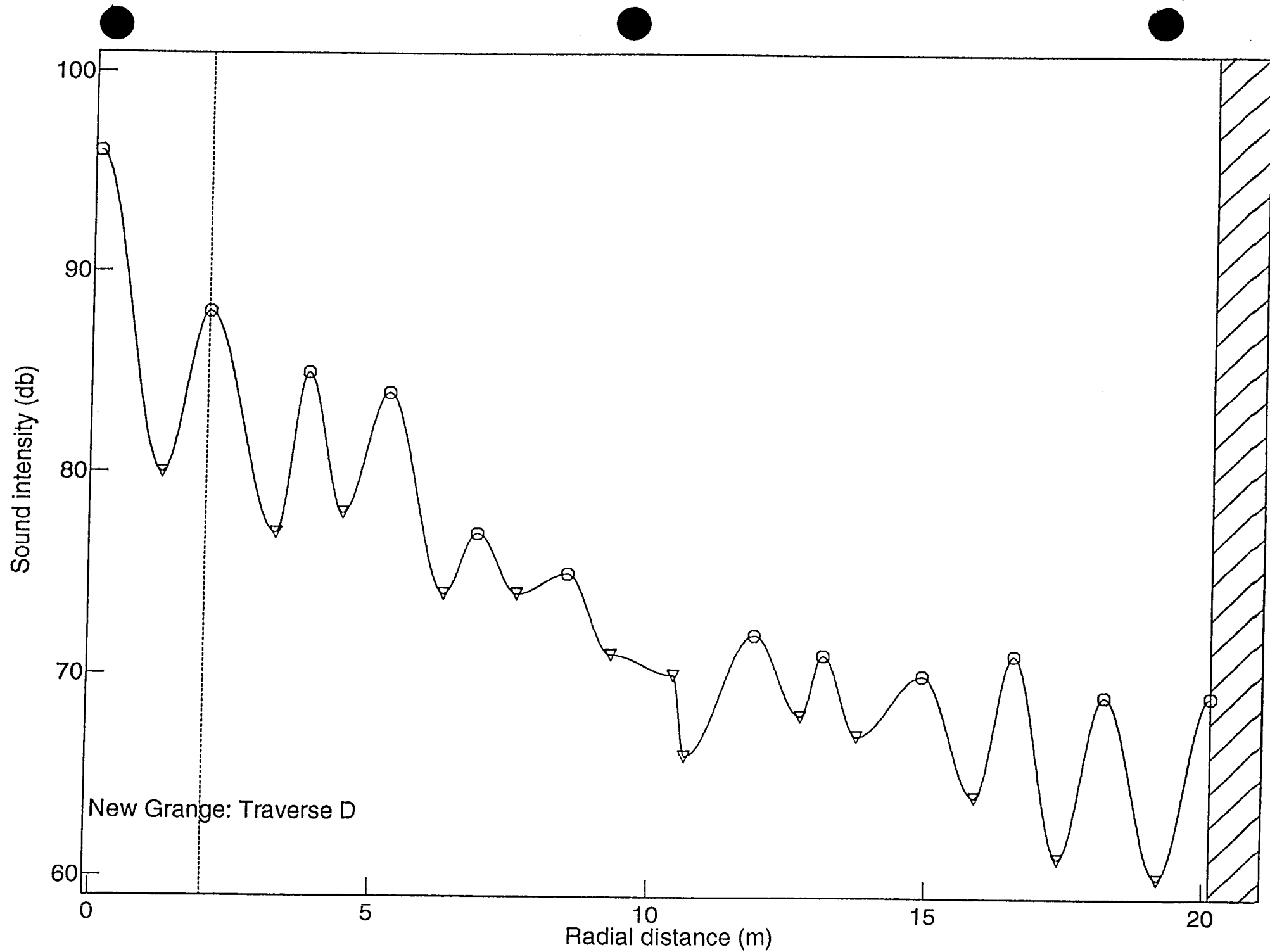




Fig. 7a - Rock Art: Newgrange Interior

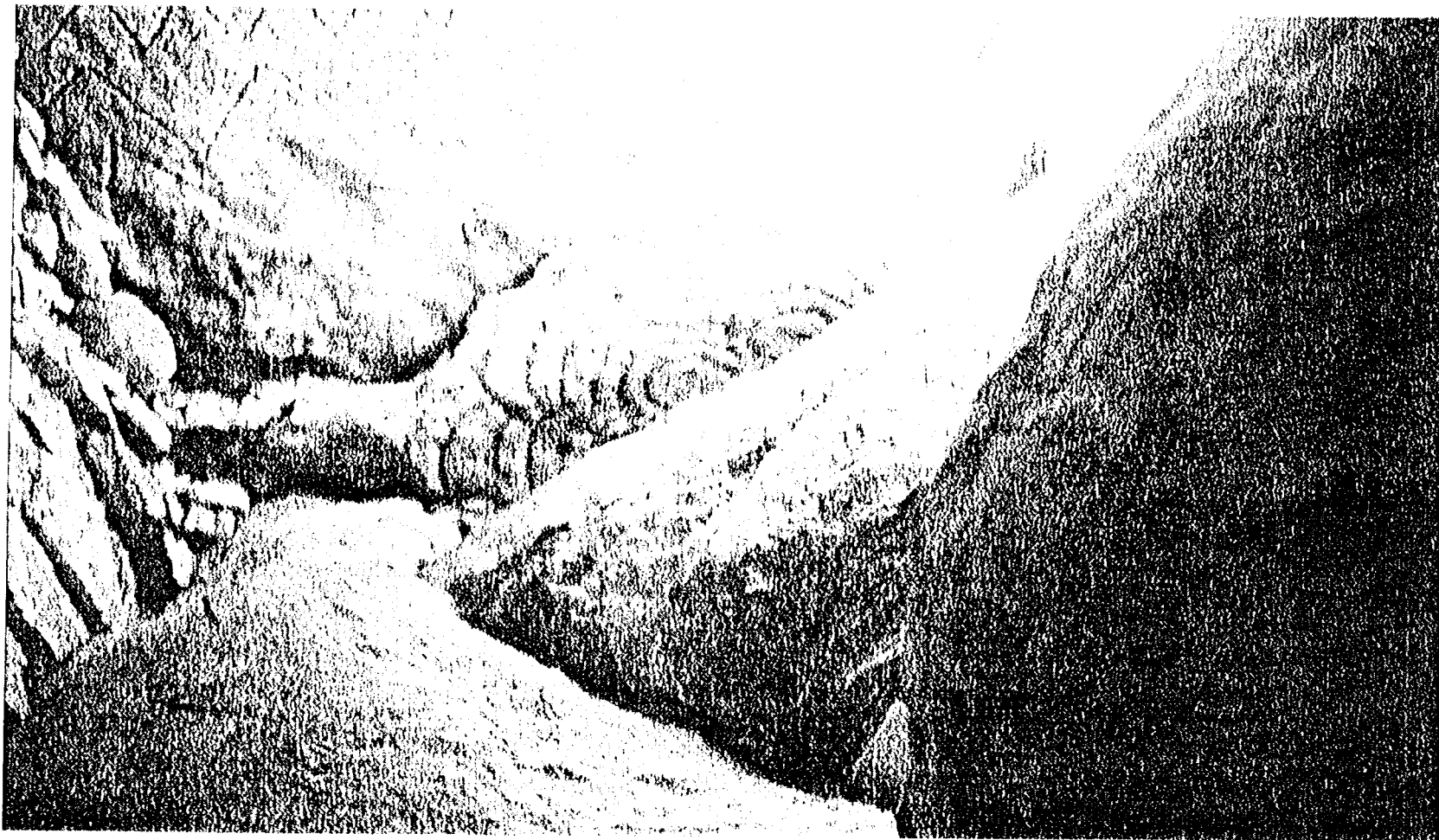


Fig. 7b - Rock Art: Newgrange Interior



Fig. 7c - Rock Art: Newgrange Interior



Fig. 7d - Rock Art: Newgrange Interior

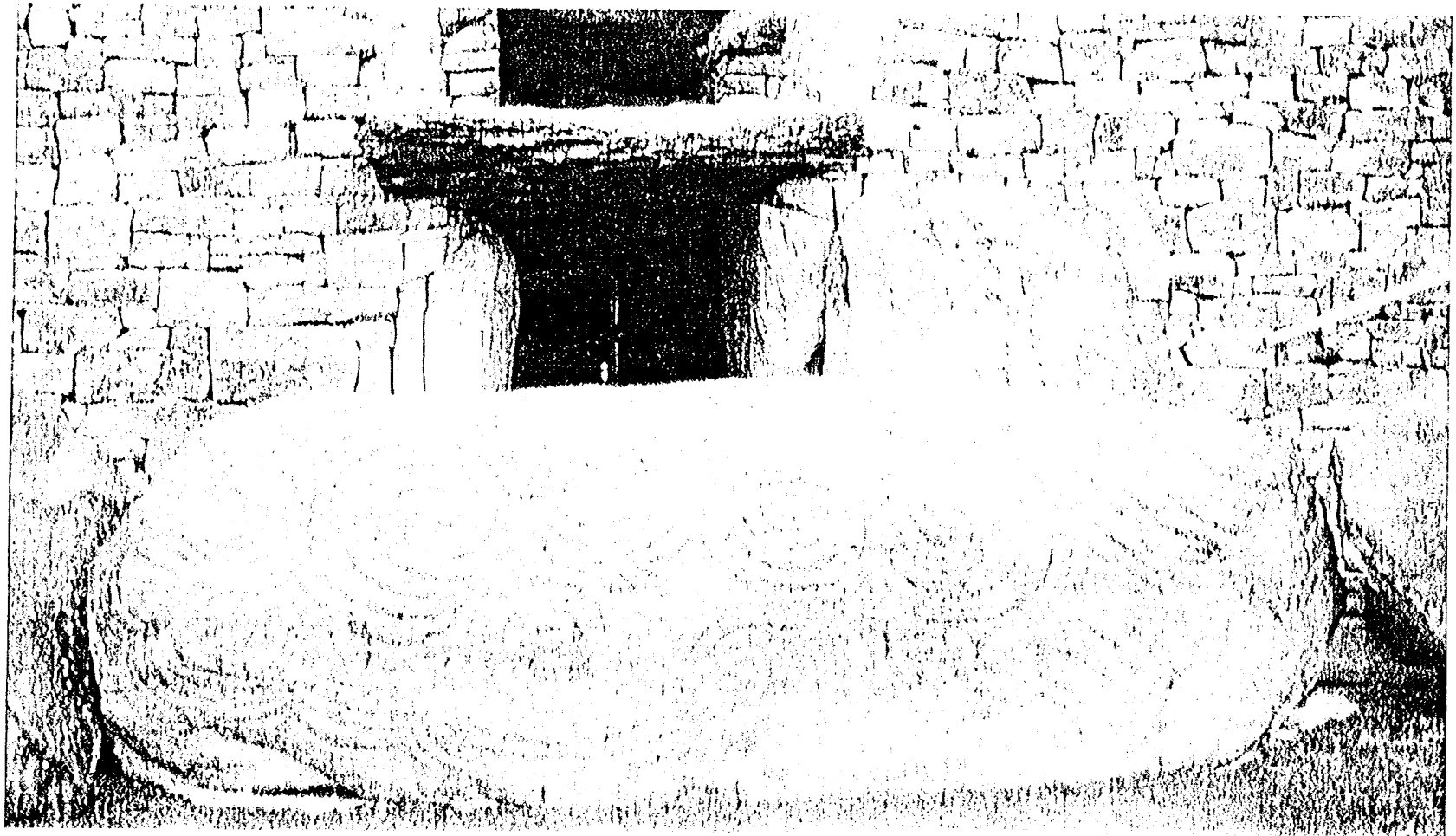


Fig. 7e - Rock Art: Newgrange Entrance Stone

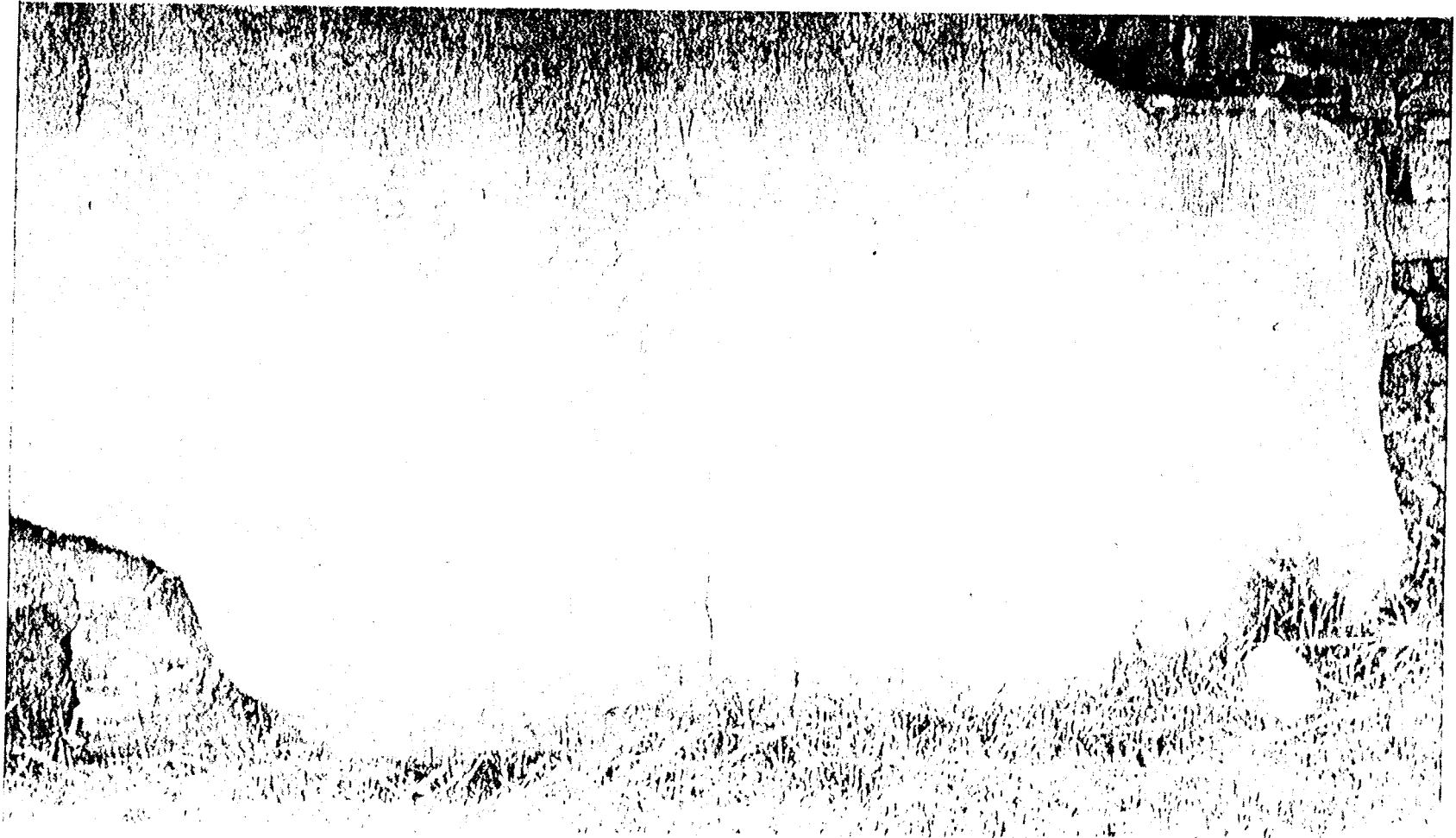


Fig. 7f - Rock Art: Newgrange Exterior Kerbstone

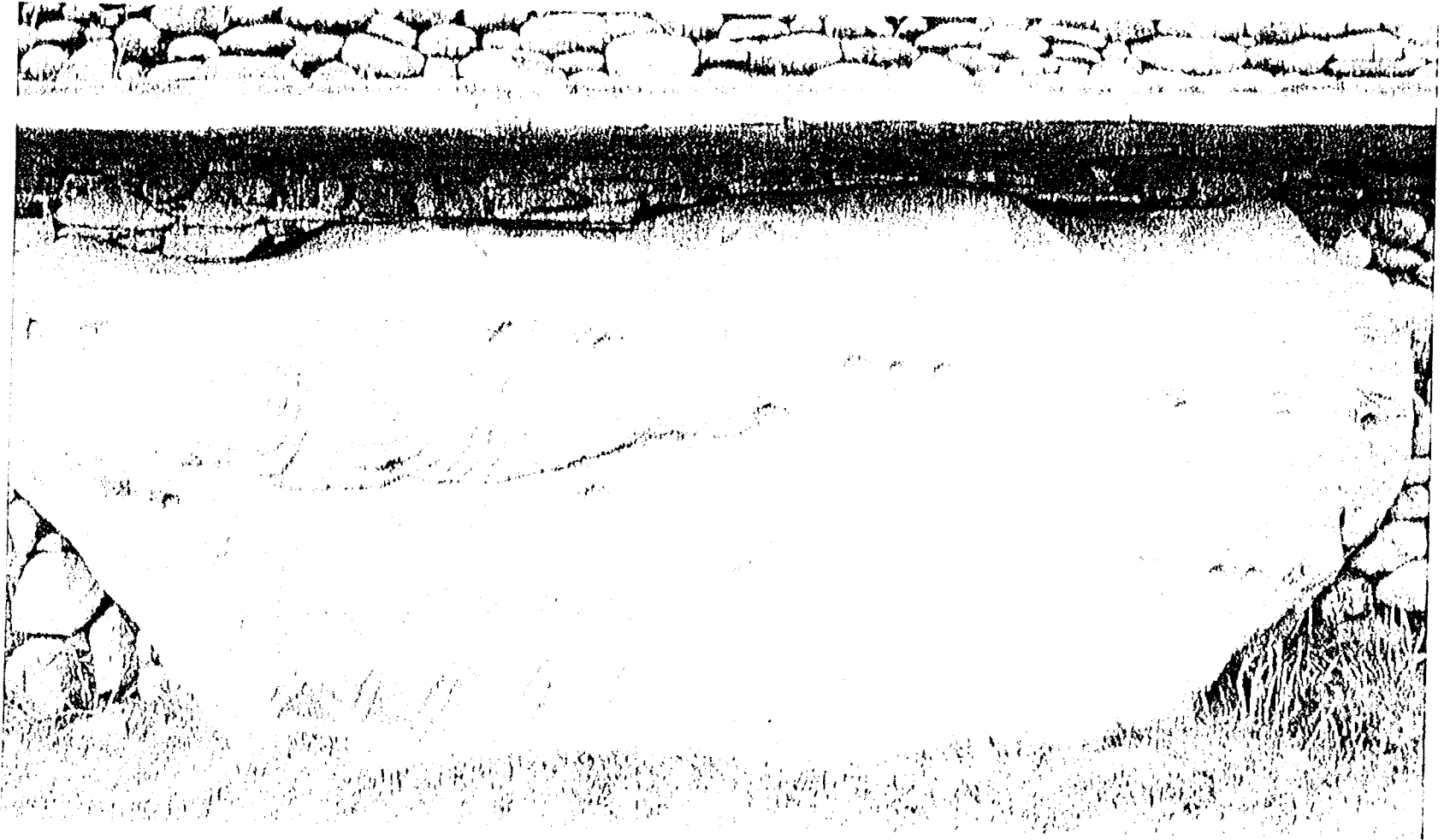


Fig. 7g - Rock Art: Newgrange Exterior Kerbstone

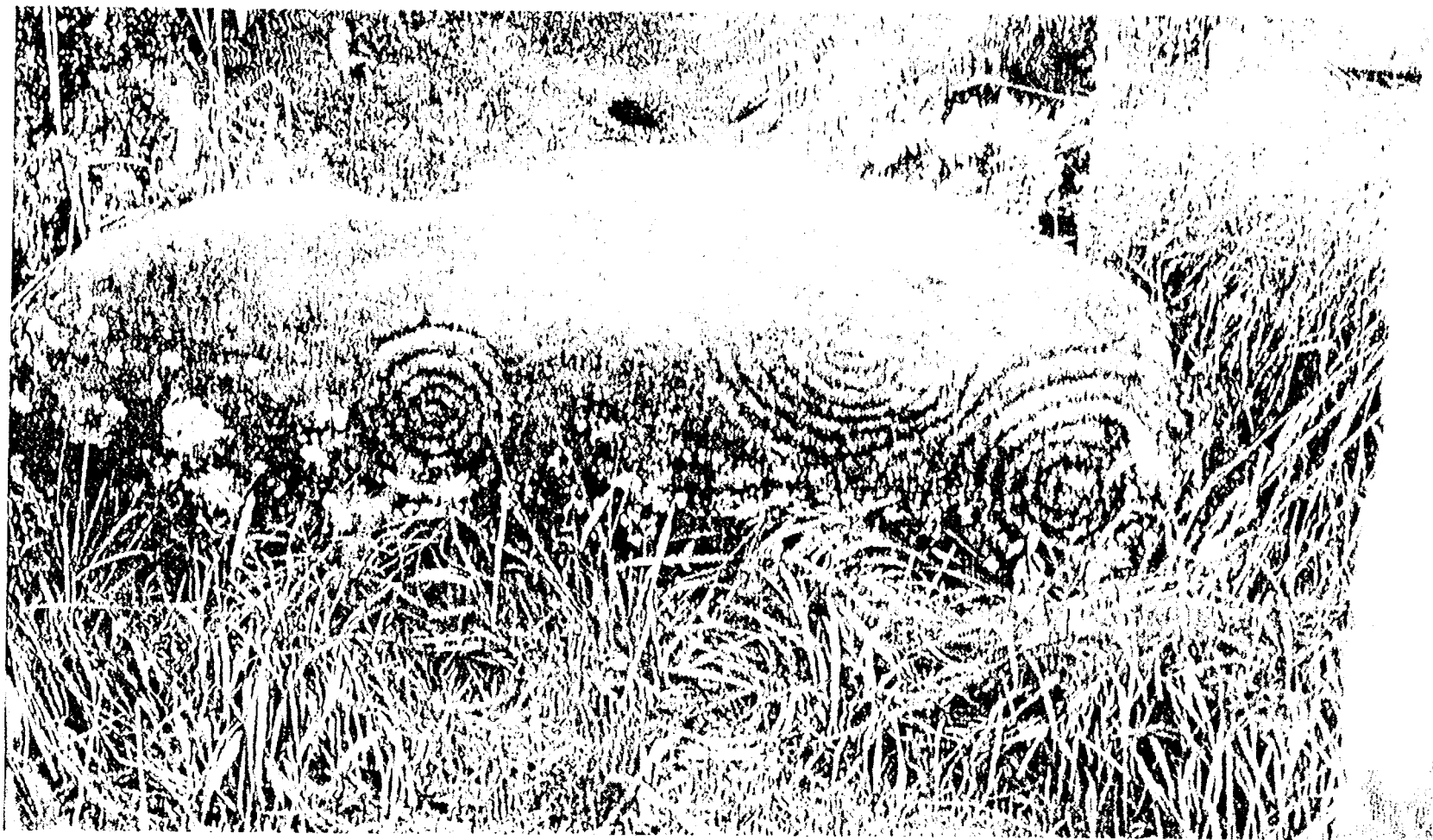


Fig. 7h - Rock Art: Loughcrew Cairn I Entrance Stone